

CHALMERS



Finite element modeling of concentration profiles and metabolism of macro-encapsulated yeast

Master of Science Thesis – Erasmus Program

GONÇALO CARVALHO ESTEVES

JOANA PAULA DA COSTA PEREIRA

Department of Chemical and Biological Engineering

Industrial Biotechnology group

CHALMERS UNIVERSITY OF TECHNOLOGY

Göteborg, Sweden, 2011

Finite element modelling of concentration profiles and metabolism of macro-encapsulated yeast

GONÇALO CARVALHO ESTEVES

JOANA PAULA DA COSTA PEREIRA

Supervisor and examiner: Associate Professor Carl Johan Franzén

Department of Chemical and Biological Engineering

Industrial Biotechnology group

Chalmers University of Technology

SE-412 96 Göteborg

Sweden

Telephone + 46 (0)31-772 1000

ACKNOWLEDGEMENT

It's hard to enumerate everyone who helped us in this path. We will refer those who had a more important role and those who have been with us, influenced positively and contributed to the development of our knowledge and personal skills.

First we would like to thank to Carl Johan Franzén, our supervisor, who guided us during the elaboration of this Master Thesis. We are grateful for his patience, for his wisdom and for being so present in these last months.

We are grateful to Claes Niclasson, for the calm and support provided in our first day in Chalmers, and for his orientation helping us to develop this project. We also would like to thank to Bengt Andersson for his enlightening explanations about CFD.

We would like to thank to Riani Lestari who provided the supportive basis to our own work.

We wouldn't be able to come to study in Gothenburg and to have such experience without the financial support of our parents. For that and for the infinite love and care, we owe them our sincere thanks.

Finally we would like to thank to our friends here in Gothenburg, the old and the recent ones, for making this period so amazing and fun and for making us feel less homesick.

ABSTRACT

With increasing energy demands and pressures on the environment, ethanol can be a more viable alternative to oil, both in an economical and environmental way.

Ethanol can be obtained from the fermentation of lignocellulosic materials. *Saccharomyces cerevisiae* has been the main subject of studies regarding this process.

The inhibitory properties of lignocellulosic fermentation media, usually lead to the reduction of yields and rates of ethanol production. Cell encapsulation may be a solution to these problems, but it might cause mass transfer problems.

To evaluate the potential benefits of macroencapsulation, concentration profiles for glucose, xylose, furfural and HMF were simulated in COMSOL Multiphysics 4.1 applying the Finite Element Method.

With the chosen kinetic parameters, xylose consumption was found to always benefit from encapsulation of cells in the presence of glucose or inhibitors. For glucose, the consumption rate was higher in the encapsulated system than with suspended yeast when the combined inhibition effect of furfural and HMF was higher than 45%.

The models formulated in this project were compared to experimental values. Generally, these models fitted the data reasonably well, after an adaptation of the q_{max} for glucose consumption.

A sensitivity analysis showed that the xylose consumption rate is generally much more sensitive than glucose reaction rate to variations in the studied parameters: maximum specific reaction rates (q_{smax}), saturation constants (K_s), inhibition constants K_{si} and diffusivities (D_{sc}).

Glucose consumption was found to be mostly sensitive to q_{gmax} and xylose consumption rate to q_{gmax} , q_{xmax} , K_x , K_{gi} and D_{gc} .

TABLE OF CONTENTS

ACKNOWLEDGEMENT	iii
ABSTRACT	iv
TABLE OF CONTENTS	v
NOMENCLATURE.....	viii
ABBREVIATIONS.....	viii
LIST OF FIGURES.....	ix
LIST OF TABLES	xi
1. INTRODUCTION	1
1.1 Purpose.....	1
1.2 Objectives.....	1
1.3 Limitations	2
2. BACKGROUND	3
2.1 Bioethanol	3
2.2 Xylose co-consumption.....	6
2.3 Inhibitors	6
2.3.1 Furans	7
2.3.2 Ethanol.....	7
2.4 Encapsulation	7
3. METHOD	9
3.1 Finite Element Method theory.....	9
3.1.1 Discretize the Continuum	9
3.1.2 Select Interpolation Functions	9
3.1.3 Find the Element Properties	9
3.1.4 Assemble the Element Properties to Obtain the System Equations	10
3.1.5 Impose the Boundary conditions	10
3.1.6 Solve the system equations.....	10
3.1.7 Make Additional Computations If Desired	10
3.2 FEM: strong and weak forms for two-dimensional mass flow	10
3.2.1 Strong form.....	11
3.2.2 Weak form	13

3.3	FE formulation of two-dimensional mass flow.....	13
3.4	Models for microbial metabolism	16
3.4.1	Model 1: Glucose consumption.....	16
3.4.2	Model 2: Glucose and Xylose co-consumption.....	16
3.4.3	Model 3: Glucose and inhibitors (furfural and HMF).....	17
3.4.4	Model 4: Glucose and Xylose co-consumption and inhibitors.....	17
3.4.5	Model 5: Glucose activation effect.....	18
3.5	Studies	18
3.5.1	Continuous fermentation	19
3.5.2	Validation	19
3.6	Assumptions.....	19
3.7	Kinetic and diffusion parameters – bibliographic revision	19
3.8	Fermentation parameters for the models.....	22
3.9	COMSOL Multiphysics	23
3.10	Simulation steps in COMSOL.....	24
3.11	COMSOL scheme for Continuous fermentation.....	25
3.12	COMSOL scheme for Validation.....	25
3.12.1	NG	25
3.12.2	G1	26
3.12.3	G2	27
3.12.4	G3	27
3.13	Mesh in COMSOL	28
4.	ANALYSIS AND DISCUSSION OF RESULTS	29
4.1	Continuous fermentation: Model 1 to 4	30
4.1.1	Concentration profiles	30
4.1.2	Dimensionless glucose plots.....	31
4.1.3	Consumption reaction plots	33
4.1.4	Efficiency factor	35
4.2	Continuous fermentation: Model 5	36
4.2.1	Concentration and reaction profiles.....	36
4.2.2	Consumption reaction plots	37

4.3	Validation	38
4.3.1	Batch cultivation of glucose	38
4.3.2	Batch cultivation of glucose and furfural	39
4.4	Sensitivity analysis	41
4.4.1	K_{si} variation effects in the consumption rate and the efficiency factor	41
4.4.2	K_{si} and D_{sc} variation effects in the efficiency factor	42
4.4.3	q_{xmax} variation effects in the efficiency factor	44
4.4.4	Control coefficient for q_{smax}	45
4.4.5	Control coefficient for K_s	46
4.4.1	Control coefficient for K_{si}	47
4.4.2	Control coefficient for D_{sc}	48
5.	CONCLUSIONS	50
6.	FUTURE WORK	51
	CONTRIBUTION REPORT	52
	REFERENCES	53
	APPENDIX	56
	APPENDIX A - Formulations	57
	APPENDIX B - Mass balance calculation	62
	APPENDIX C - Determination of the average volume around each sphere	63
	APPENDIX D - Determination of the relation between diffusion and the cell growth inside the cell pellet for G2	64
	APPENDIX E - Determination of the growth equation	65
	APPENDIX F - Determination of movement velocity of the cell pellet boundary	67
	APPENDIX G - Control coefficient	69

NOMENCLATURE

f – Furfural

g – Glucose

h – 5-hydroxymethylfurfural

s – General designation for substrates or inhibitors

x – Xylose

ABBREVIATIONS

COMSOL – COMSOL Multiphysics 4.1

HMF – 5-hydroxymethylfurfural

LIST OF FIGURES

<i>Figure 1. Main products of the hydrolysis process of the lignocellulosic materials. Adapted from [10].</i>	5
<i>Figure 2. Metabolic pathway of ethanol fermentation by <i>Saccharomyces cerevisiae</i>. Adapted from [11].</i>	5
<i>Figure 3. Xylose metabolic pathways. Adapted from [12].</i>	6
<i>Figure 4. Inhibition mechanisms of furans, weak acids and phenolic compounds in <i>Saccharomyces cerevisiae</i>. Adapted from [13].</i>	7
<i>Figure 5. Steps of the formulation process in COMSOL.</i>	24
<i>Figure 6. 2D geometry in COMSOL simulating the Capsule structure: 1- Membrane; 2- Cell pellet and 3- Liquid core.</i>	25
<i>Figure 7. 2D COMSOL geometry for the batch simulation for model 1 and 3 (without HMF): 1- Average medium volume; 2- Membrane; 3- Cell pellet and 4- Liquid core.</i>	26
<i>Figure 8. 2D Geometry in COMSOL. Case of the growth inside half sphere. 1- Average medium volume; 2- Membrane; 3- Cell pellet and 4-Liquid core.</i>	26
<i>Figure 9. 2D Geometry for the cell growth simulation for the entire capsule filled with cells. 1- Average medium volume; 2- Membrane and 3- Cell pellet.</i>	27
<i>Figure 10. 2D Geometry in COMSOL - moving boundary. 1- Average medium volume; 2- Membrane; 3- Liquid core and 4- Cell pellet.</i>	27
<i>Figure 11. Options taken in the process of Mesh creation in COMSOL.</i>	28
<i>Figure 12 Profile concentrations of substrates and inhibitors for models 1 to 4.</i>	30
<i>Figure 13. Cut line 2D in COMSOL.</i>	31
<i>Figure 14. Profiles of dimensionless glucose concentration in the dimensionless radial coordinate.</i>	32
<i>Figure 15. Dimensionless concentrations of substrates and inhibitors along the dimensionless radial coordinate for model 4.</i>	32
<i>Figure 16. Uptake kinetics for glucose, xylose, furfural and HMF in model 4.</i>	33
<i>Figure 17. Xylose consumption rate through the time for model 2 and for model 4.</i>	33
<i>Figure 18. a. Glucose concentration profile (mol/m^3); b. Xylose concentration profile (mol/m^3); c. Glucose consumption rate profile ($\text{mol}/(\text{m}^3 \text{ s})$); d. Xylose consumption rate profile ($\text{mol}/(\text{m}^3 \text{ s})$), for time = 660 s in model 4.</i>	34
<i>Figure 19. a. Glucose concentration profile (mol/m^3); b. Xylose concentration profile (mol/m^3); c. Glucose consumption rate profile ($\text{mol}/(\text{m}^3 \text{ s})$); d. Xylose consumption rate profile ($\text{mol}/(\text{m}^3 \text{ s})$), for time = 86400 s in model 5.</i>	36

<i>Figure 21. Xylose consumption rate as a function of glucose concentration along the cut line.</i>	37
<i>Figure 20. Cut line 2D in COMSOL for glucose activation effect plot (blue line).</i>	37
<i>Figure 22. Comparison of glucose batch simulations with experimental values from Talebnia et al [35].</i>	39
<i>Figure 23. Concentration of glucose in batch fermentation with furfural [5 g/L]. In black are the results obtained by Talebnia et al [35].</i>	40
<i>Figure 24. Concentration of Furfural in batch fermentation with glucose [40 g/L]. The line in black are the results obtained by Talebnia et al [35].</i>	40
<i>Figure 25. η versus k. Parametric sweep results for testing different values of K_{si} for furfural and HMF.</i>	42
<i>Figure 26. Representation of the variation of η for xylose, when K_{si} and D_{sc} are changed. The distance for the center represents the axis for η, the extreme points of the pentagon are the values of k and the legend of the series stands for the values of b.</i>	43
<i>Figure 27. Representation of the variation of η for glucose, when K_{si} and D_{sc} are changed. The distance for the center represents the axis for η, the extreme points of the pentagon are the values of k and the legend of the series stands for the values of b.</i>	43

LIST OF TABLES

<i>Table 1. Lignocellulosic sources' composition (% dry weight), adapted from [5]</i>	4
<i>Table 2. Diffusion coefficients for the fermentation substrates and inhibitors</i>	20
<i>Table 3. Kinetic parameters for glucose, xylose, furfural and HMF consumption by <i>Saccharomyces cerevisiae</i> – bibliography review</i>	21
<i>Table 4. Kinetic and diffusion values for the models 1 to 5</i>	22
<i>Table 5. Efficiency factor for glucose, xylose, furfural and HMF in the models</i>	35
<i>Table 6. k and respective values for the inhibition constants. k equal to 1 corresponds to the values of K_{si} used in the initial formulation</i>	41
<i>Table 7. b and respective values for the diffusion coefficients in the cell pellet. b equal to 1 corresponds to the values of D_{sc} used in the initial formulation</i>	42
<i>Table 8. m and the values for the maximum xylose consumption rate constant. m equal to 1 corresponds to the values of q_{xmax} used in the initial formulation</i>	44
<i>Table 9. Values of glucose reaction rate and efficiency factor for different values of m</i>	44
<i>Table 10. Reaction rate and efficiency factor for xylose consumption for m values</i>	44
<i>Table 11. Control coefficient of q_{smax} over $-r_g$</i>	45
<i>Table 12. Control coefficient of q_{smax} over $-r_x$</i>	45
<i>Table 13. Control coefficient of K_s over $-r_g$</i>	46
<i>Table 14. Control coefficient of K_s over $-r_x$</i>	46
<i>Table 15. Control coefficient of K_{si} over $-r_g$</i>	47
<i>Table 16. Control coefficient of K_{si} over $-r_x$</i>	47
<i>Table 17. Control coefficient of D_{sc} over $-r_g$</i>	48
<i>Table 18. Control coefficient of D_{sc} over $-r_x$</i>	48
<i>Table 19. Tasks and the respective participation of the master's students, (-) stands for less participative and (+) for more</i>	52

“No matter how complicated a problem is, it usually can be reduced to a simple, comprehensible form which is often the best solution.”

An Wang

1. INTRODUCTION

Bioethanol is one of the new materials that is appointed as a promising huge support for the transition between fossil fuels to renewable and sustainable fuels. This change can be an answer to world big issues such as oil depletion and oil market fluctuations, energy needs, resource depletion, greenhouse effect, global warming, biodiversity and land destruction. Because these problems are all correlated to population growth, this change might be a big step towards a sustainable, economic and environmental life style [1][2].

Conventional oil has already achieved its peak of production, and it is now in decline (statistically it will end in the 2090 decade – Hubbert Curve) [1]. Bioethanol emerges as a progressive, economic and sustainable alternative to the fossil fuels, which production and consumption market are increasing every year [2][3] encouraged also by the biofuel support policies adopted in recent times by the US (until 2022 it will achieve 60 billion liters of second-generation biofuels) and the UE (by 2020 the transport sector will represent to us 10% of renewable energy) [4].

The research on improving bioethanol productivity is important to make it more competitive. The productivity depends on various factors, one of which is the presence of inhibitors in the composition of the fermentation medium [5]. Encapsulation of cells for ethanol fermentation has been the subject of several studies and developments to overcome the inhibition effects of those compounds [5].

1.1 Purpose

This projects aims to obtain concentration profiles inside the capsules for glucose, xylose and inhibitors, taking into account the cell growth. The achievement of these profiles can lead to improvements on the knowledge of the local conditions and cell behavior inside the capsules. This can be an important tool in the optimization of fermentation processes with immobilized microorganisms.

The models formulated to obtain the profiles should be realistic and should be able to fit experimental data for similar situations.

1.2 Objectives

The objectives of this Master Thesis project are listed below:

- i. To formulate models that describe microbial kinetics and mass diffusion of encapsulated yeast;
- ii. To simulate concentration profiles of glucose, xylose and inhibitors within the capsule with entrapped yeast population using COMSOL Multiphysics 4.1;
- iii. To study the effect of the biomass growth;
- iv. To analyze the model's capability to recreate published data;
- v. To analyze the sensitivity of the modeling results to the parameter values.

1.3 Limitations

In order to decrease the required computation, the domain chosen was the 2D with axisymmetry applied. This is consistent with previous studies of Riani Lestari [6].

To reduce the use of parameters and variables, the formulation was defined as simple black box models. The equations for the biodegradation processes were based on the Monod model.

2. BACKGROUND

2.1 Bioethanol

Ethanol is an alcohol, C_2H_5OH , obtained through petrochemical processes – synthetic ethanol – or through fermentative process of carbohydrates compounds – bioethanol. There is an enormous set of different raw materials that can be used as a carbohydrate source: lignocellulosic materials (wood, straw, bagasse), starch materials (wheat, rice, corn, maize) and sugar materials (sugar cane, sugar beets) [5][7]. However, the lignocellulosic materials are the most promising because of their high sustainable and environmental potential:

- Largest renewable carbohydrate source;
- Environmental pathways to industrial and agricultural residues;
- Clean up of lands vegetation;
- Decreasing of residues and GHG emissions;
- Globalization of bioethanol market;
- No interference with food industry (feedstocks).

Some studies are being made to spread this demand of carbohydrate sources from the oceans, essentially, algae (seaweeds) and animal skeleton biomass [5].

The lignocellulosic materials are essentially woody materials from forests and crops residues which have mostly hemicellulose, cellulose and lignin, in their composition - *Table 1*. Only the two first ones can be converted by hydrolysis to sugars – lignocellulosic hydrolysates -and then used as substrates in the fermentation process [7][8].

Before the hydrolysis of the cellulosic compounds, a pretreatment is performed to remove some resistant materials to hydrolytic process. It can be a physical, physicochemical, chemical or biological process. The most commonly applied to lignocellulosic materials are the dilute-acid, SO_2 and steam explosion methods [7][9].

In the hydrolysis process, cellulolytic enzymes are used to degrade cellulose to cellobiose and then to glucose, destroying the chemical bonds between lignin-cellulose and lignin-hemicellulose, and producing an optimized substrate to the next processes.

The main products of the hydrolysis of the lignocellulosic materials are represented in *Figure 1*: sugars (top) and inhibitors (bottom).

The hydrolysis process is then followed by the alcoholic fermentation, a process in which the sugars are consumed by microorganisms, and, simultaneously, CO_2 and ethanol are formed as products of the reaction [10].

Table 1. Lignocellulosic sources' composition (% dry weight), adapted from [5]

Biomass or waste	Cellulose	Hemicellulose	Lignin
Trees			
Poplar	45-50	17-19	18-26
Eucalyptus	50	13	28
Pine (spruce)	44	23	28
Salix (hardwood)	43	22	26
Grasses			
Switchgrass	31-45	20-30	12-18
Bermuda grass	25	36	6
Rye grasses	25-40	35-50	10-30
Paper			
Office paper	69-99	0-12	0-15
Newspaper	40-55	25-40	18-30
Paper pulp	60-70	10-20	5-10
Food/agriculture wastes			
Corn cobs	45	35	15
Corn stover	38-40	22-28	18-23
Corn fibre	14	17	8
Wheat straw	30-38	21-50	15-23
Rice husk	24	27	13
Bagasse	38	27	20
Nut shells	25-30	25-30	30-40
Leaves	15-30	80-85	0
Cattle manure	1.6-4.7	1.4-3.3	2.7-5.7
Other wastes			
Sorted refuse	60	20	20
Primary	8-15	NA	24-29
Wastewater			
solids	33	9	17
Municipal solid waste (MSW)	62	5	11
MSW paper pulp			

This reaction can be performed by many species of yeast such as *Saccharomyces cerevisiae*, *Pichia stipitis*, *Kluveromyces marxianus*, and species of bacteria such as *Zymomonas mobilis* and *Escherichia coli*. All these microorganisms were studied for bioethanol production, however, *Saccharomyces cerevisiae* is the predominantly species used in this industrial processes. In *Figure 2* is represented the glucose pathway of *Saccharomyces cerevisiae* [11]

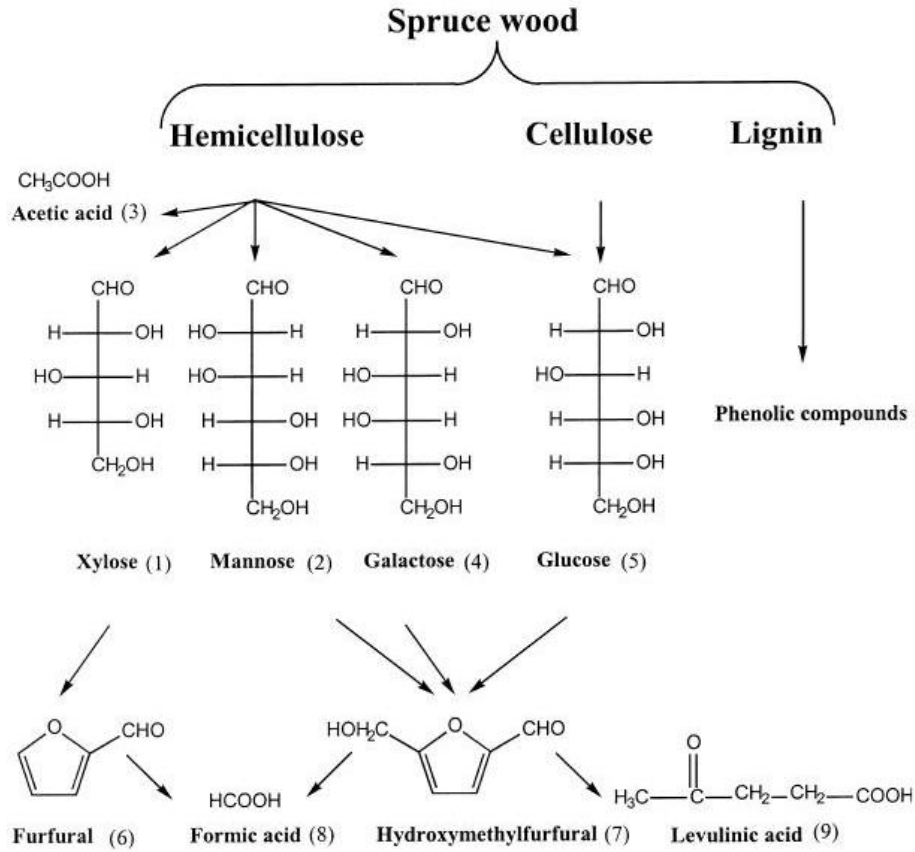


Figure 1. Main products of the hydrolysis process of the lignocellulosic materials. Adapted from [10].

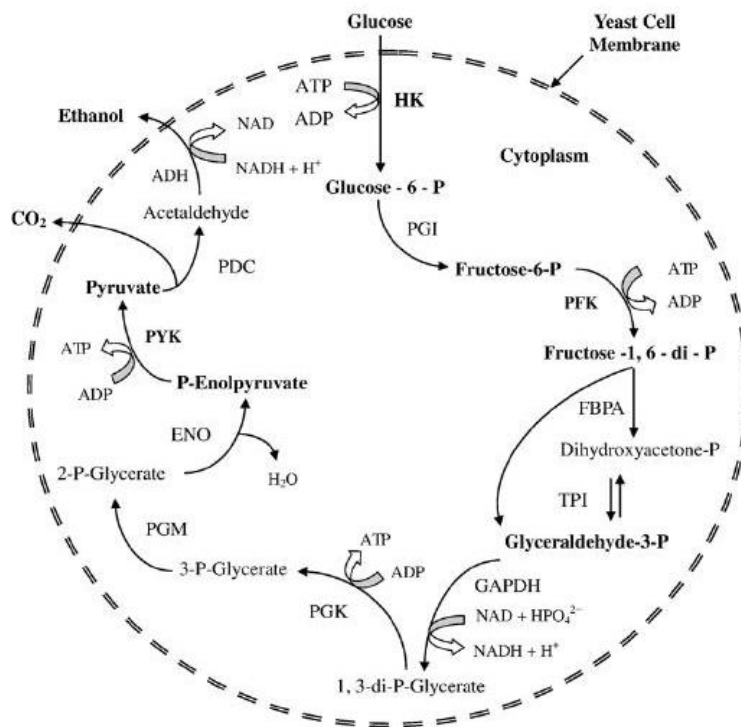


Figure 2. Metabolic pathway of ethanol fermentation by *Saccharomyces cerevisiae*. Adapted from [11].

2.2 Xylose co-consumption

Saccharomyces cerevisiae is only able to degrade hexoses (glucose, mannose and galactose), so the pentoses (xylose, arabinose) consumption represents an issue in this process. There are several strategies to overcome this problem such as the use of a co-culture of microorganisms or genetically modified microorganisms (incorporation of genes from other species or changes in their metabolic pathways) [5].

In this project xylose and glucose will be the substrates used in the fermentation process carried out by a genetically engineered *Saccharomyces cerevisiae* strain. *Figure 3*, shows the xylose metabolic pathways [12].

2.3 Inhibitors

The cultivation medium for fermentation is usually filled with various substances with inhibitory character. This represents an opposition to yeast maximum productivity. As the aim is to achieve maximum production with less fermentation time, it becomes imperative to minimize the inhibitory effects on the cells, *Figure 4*.

The inhibitors in the lignocellulosic hydrolysates can be divided in groups. First are the substances liberated during the processes of prehydrolysis and hydrolysis. In this group are the acetic acid and extractives such as terpenes, alcohols and some aromatic compounds [8].

In the second group we can find the inhibitors produced as byproducts during prehydrolysis and hydrolysis as a result of sugars' degradation. These are furfural, HMF (5-hydroxymethylfurfural), levulinic acid, formic acid and humic substance [8].

Thirdly are a variety of aromatic and polyaromatic compounds, products that result of lignin degradation. In the fourth group are the products of the fermentation process such as ethanol, glycerol, lactic acid and acetic acid [8].

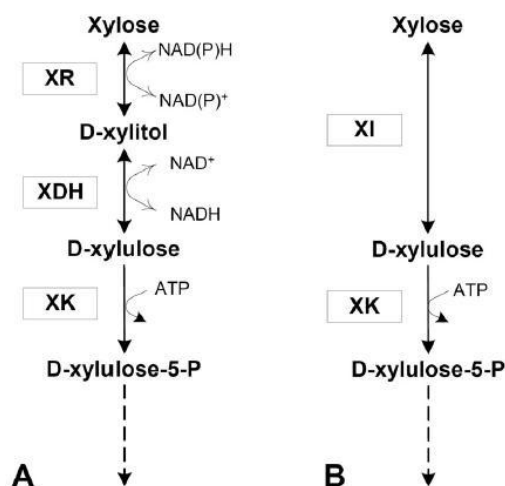


Figure 3. Xylose metabolic pathways. Adapted from [12].

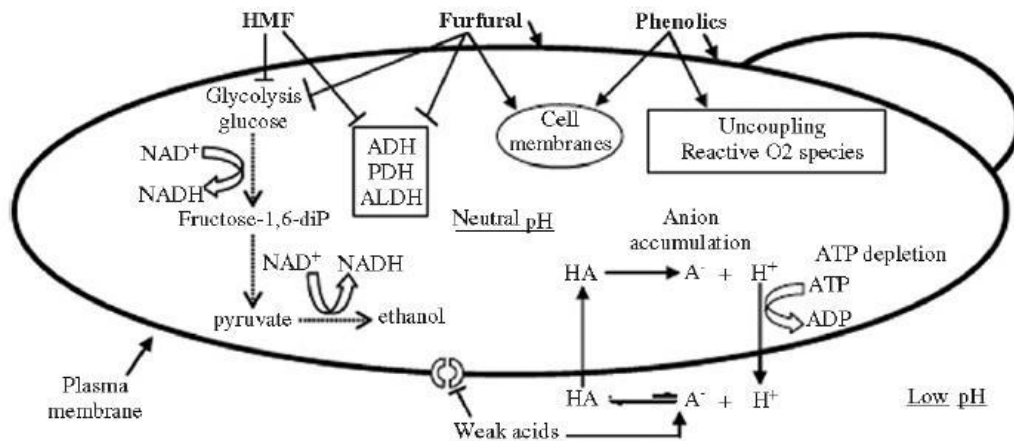


Figure 4. Inhibition mechanisms of furans, weak acids and phenolic compounds in *Saccharomyces cerevisiae*. Adapted from [13].

2.3.1 Furans

Furans affects the direction of energy used by yeast - reduction of ATP and NAD(P)H intracellular concentrations - in order to remediate their alterations in the cells [13]. It will result in the reduction of volumetric ethanol yield and productivity, the inhibitory effect on the cell growth and the enlargement of the lag phase [10].

2.3.2 Ethanol

The ethanol effect on the cells results in changes in the intracellular metabolism of the cells. Both cell growth and ethanol productivity are affected. The ethanol inhibitory effects could be related to its influence on some enzymes such as hexokinase and ADH. Ethanol could also contribute to alterations in the activity of ATPase which will modify the nutrient uptake and membrane potential [10].

2.4 Encapsulation

The production of bioethanol from lignocellulosic materials has some unconventional byproducts that decrease the ethanol yield: acetic acid, phenolic compounds, furfural and HMF. Even the accumulation of ethanol acts as an inhibitor for cells growth. The substrate limitation, osmotic pressure, pH, temperature are other stress factors that decrease the cell efficiency and viability [10][11].

Several techniques have been tested to improve the cell resistance to inhibition factors; however, the encapsulation method has the highest balance between productivity, cost and simplicity. The most used and studied immobilization methods are the encapsulation of yeasts in a matrix and the encapsulation in spheres capsules – both as macro-encapsulation [11].

In this project, alginate spheres with liquid core to immobilize and protect the yeasts during the bioethanol production will be studied. Although the alginate capsule confers protection against some inhibitors, there are some consequences that could decrease the efficiency of the process, mostly caused by mass diffusivity through the capsule membrane.

Substrate and ethanol diffusivities, and the decreasing of space available to cells growth, are some of the issues that are currently analyzed and studied to optimize biomass growth and the ethanol yield [11].

3. METHOD

In order to be able to describe the concentration profiles of substrates and products, as well as the cell growth, modeling work was made in COMSOL Multiphysics 4.1, applying FEM (Finite Element Method).

3.1 Finite Element Method theory

The Finite Element Method is a mathematical approach in which a continuum problem can be solved by dividing the solution domain into smaller elements. These elements – finite elements - have the same properties of those who originated them but they are simpler to define and to reduce the number of unknowns [14].

The division results in elements composed by edges and nodes which are points of interception and connection between elements.

The solution of differential equations regarding the physical problem can be solved by approximated functions that satisfy the conditions described by integral equations in the problem domain. These approximated functions are usually polynomial functions [14].

In FEM there are two ways to solve problems described as partial differential equations. The so-called "strong form" is the direct resolution of the equations. The "weak form" has evolved from approximated numerical methods that are integral representations of differential equations governing the physical problem. The "strong form" requires continuity in the solution of dependent variables so it's more difficult to work with it. The "weak form" allows a unique method to solve different types of problems because the methods to transform differential equations in an integral form are generics that usually provide more precise results. Due to its advantages in complex geometries it is the most used form [15].

The general steps of the Finite Element Method [14] are described as follows.

3.1.1 Discretize the Continuum

The first step consists in the division of the body in small elements. The type, size and number of elements are in the field of the engineer judgment but can be supported with research.

3.1.2 Select Interpolation Functions

Next step is to choose interpolation functions. It is defined in the element using the nodal values of the element. The most common functions are linear, quadratic and cubic polynomials, because they are simple to work with. The degree of the polynomial varies according to the number and nature of nodes of the elements and the unknowns at each node.

3.1.3 Find the Element Properties

The following step is to set the matrix equations. For this, various methods can be used. In this project the weak form has relevance, therefore it will be the approach used.

3.1.4 Assemble the Element Properties to Obtain the System Equations

In order to obtain the final and global equation for the system, the next step is to collect and assemble the equations for the element proprieties.

3.1.5 Impose the Boundary conditions

Previously to solving the system of equations, the equations have to be changed so that it can regard the boundary conditions.

3.1.6 Solve the system equations

The assemblage results in a group of equation with n unknown nodal values - degrees of freedom. The kind of equations to be solved depends on the type of problem and if it is time dependent or not.

3.1.7 Make Additional Computations If Desired

In the end, other parameters dependent of those calculated can be also obtained. It can also be important to determine at what position deformations and large stresses occur.

3.2 FEM: strong and weak forms for two-dimensional mass flow

It has already been said that the weak form is the base for FEM. In the next lines, the procedure to pass from the strong form to the weak form is going to be described [16].

Fick's law applied to one dimension problems gives the quantity of mass circulating through a unit area per unit of time:

$$N = -D \frac{dC}{dx} \quad (1)$$

Now, in problems for two-dimensional, considering that the mass flux will be in more than one direction, it has to be included the mass flux vector, \mathbf{j} .

$$\mathbf{j} = \begin{bmatrix} j_x \\ j_y \end{bmatrix} \quad (2)$$

This vector with the units of $mol/(m^2s)$ has the same direction of the mass flow, and its length represents the mass per unit time per unit of area perpendicular to the direction of mass flow. The unit vector n normal to the boundary has to be considered too.

$$\mathbf{n} = \begin{bmatrix} n_x \\ n_y \end{bmatrix} \quad (3)$$

Now the objective is to obtain the value of j_n , designed by flux, that is the quantity of mass passing through a unit of area of the boundary per unit of time.

$$j_n = j^T n \quad (4)$$

The Fick's law can be written:

$$j = -E \nabla C \quad (5)$$

With:

$$\nabla C = \begin{bmatrix} \frac{\partial C}{\partial x} \\ \frac{\partial C}{\partial y} \end{bmatrix} \quad (6)$$

And E being the constitutive matrix, which can be interpreted as the easiness that each particular solute moves in a particular mean.

$$E = \begin{bmatrix} D_{xx} & D_{xy} \\ D_{yx} & D_{yy} \end{bmatrix} \quad (7)$$

Considering E symmetric:

$$E = E^T \quad (8)$$

3.2.1 Strong form

Considering the existence of an amount J , that refers to the quantity of mass going into the body per unit of volume and time ($J/(m^3 s)$), in stationary problems we have:

$$\int_A J t dA - \int_A R dA = \oint_L j_n t dL \quad (9)$$

where R is the rate of consumption of substrate and t - equal to $t(x, y)$ - is the thickness of the body in the z-axis.

From equation (4), it can be written:

$$\oint_L t j_n dL = \oint_L t j^T n dL = \oint_L (tj)^T n dL = \int_A \text{div}(tj) dA \quad (10)$$

$$\int_A [tJ - tR - \text{div}(tj)] dA = 0 \quad (11)$$

Considering the arbitrary of region A arbitrary:

$$\text{div}(tj) = tJ - tR \quad (12)$$

If the thickness of the body (t) is constant:

$$\text{div}(j) = J - R \quad (13)$$

and knowing that the divergent of j is:

$$\text{div}(j) = \frac{\partial j_x}{\partial x} + \frac{\partial j_y}{\partial y} \quad (14)$$

using the Eq. (5) and applying it to Eq. (13), in Region A we get:

$$\text{div}(tE\nabla C) + tJ - tR = 0 \quad (15)$$

Considering that the diffusivity is the same in all directions (isotropic materials):

$$E = D \begin{bmatrix} 1 & 0 \\ 0 & 1 \end{bmatrix} \quad (16)$$

The Eq. (15) will become:

$$\frac{\partial}{\partial x} \left(tD \frac{\partial C}{\partial x} \right) + \frac{\partial}{\partial y} \left(tD \frac{\partial C}{\partial y} \right) + tJ - tR = 0 \quad (17)$$

If tD is constant,

$$\frac{\partial^2 C}{\partial x^2} + \frac{\partial^2 C}{\partial y^2} + \frac{J}{D} - \frac{R}{D} = 0 \quad (18)$$

In order to solve this, boundary conditions should be defined. The most usual are:

$$j_n = j^T n = h \text{ on } L_h \quad (19)$$

$$C = g \text{ on } L_g \quad (20)$$

L_h is the boundary part of L , where the mass flux is known, h ; and L_g is the boundary part of L where the concentration C is the value g .

Summarizing:

Strong form of two-dimensional mass flow:

$$\text{div}(tE\nabla C) + tJ - tR = 0 \quad (21)$$

$$j_n = j^T n = h \text{ on } L_h \quad (22)$$

$$C = g \text{ on } L_g \quad (23)$$

3.2.2 Weak form

To obtain the weak form, the balance principle for two-dimensional body, Eq. (15) must be multiplied by an arbitrary function v equal to $v(x, y)$ - the weight function - and then we integrate over the A .

$$\int_A v \operatorname{div}(jt) dA - \int_A v Jt dA + \int_A v Rt dA = 0 \quad (24)$$

Applying the Green-Gauss theorem we get:

$$\int_A v \operatorname{div}(jt) dA = \oint_L vtj^T n dL - \int_A (\nabla v)^T jt dA \quad (25)$$

Then the Eq. (24) becomes:

$$\int_A (\nabla v)^T jt dA = \oint_L vtj^T n dL - \int_A v Jt dA + \int_A v Rt dA \quad (26)$$

And using the boundary conditions we obtain:

$$\int_A (\nabla v)^T E \nabla C t dA = - \int_{L_h} v h t dL - \int_{L_g} v j_n t dL + \int_A v Jt dA - \int_A v Rt dA \quad (27)$$

$$C = g \text{ on } L_g \quad (28)$$

3.3 FE formulation of two-dimensional mass flow

The following equations define the FE formulation for two-dimensional mass flow problems [16]. The concentration of specie C , can be approximated by:

$$C = Ma \quad (29)$$

being M the global shape function matrix and a the matrix containing the concentrations in each node. As it shows:

$$M = [M_1 \quad M_2 \quad \dots \quad M_n]; \quad a = \begin{bmatrix} C_1 \\ C_2 \\ \vdots \\ C_n \end{bmatrix} \quad (30)$$

where n is the number of nodes of the body.

Considering now a variable B , that:

$$\nabla C = Ba \quad \text{where} \quad B = \nabla M \quad (31)$$

$$B = \begin{bmatrix} \frac{\partial M_1}{\partial x} & \frac{\partial M_2}{\partial x} & \cdots & \frac{\partial M_n}{\partial x} \\ \frac{\partial M_1}{\partial y} & \frac{\partial M_2}{\partial y} & \cdots & \frac{\partial M_n}{\partial y} \end{bmatrix} \quad (32)$$

Combining Eq. (27) with Eq. (31):

$$\left(\int_A (\nabla v)^T E B t dA \right) a = - \int_{L_h} v h t dL - \int_{L_g} v j_n t dL + \int_A v J t dA - \int_A v R t dA \quad (33)$$

The last step is to decide the arbitrary function v according to the Galerkin method:

$$v = M c \quad (34)$$

The matrix c is arbitrary too, so

$$\nabla v = B c \quad (35)$$

As v is symmetric:

$$v = c^T M^T \quad (36)$$

Replacing the three previous equations in Eq. (33), and considering that c doesn't depend on the position, we get:

$$\left(\int_A B^T E B t dA \right) a = - \int_{L_h} M^T h t dL - \int_{L_g} M^T j_n t dL + \int_A M^T J t dA - \int_A M^T R t dA \quad (37)$$

To make it simple and understandable, the following matrices are defined as:

$$\begin{aligned} K &= \int_A B^T E B t dA \\ f_b &= - \int_{L_h} M^T h t dL - \int_{L_g} M^T j_n t dL \\ f_l &= \int_A M^T J t dA \\ f_r &= - \int_A M^T R t dA \end{aligned} \quad (38)$$

f_b is called the boundary vector, f_l the load vector and f_r the reaction vector. Ka can be written as:

$$Ka = f_b + f_l + f_r \quad (39)$$

And the force vector can be written as:

$$f = f_b + f_l + f_r \quad (40)$$

So:

$$Ka = f \quad (41)$$

Now, considering the force vector as:

$$f_i = f_{bi} + f_{li} + f_{ri}; \quad i = 1, \dots, n \quad (42)$$

As a consequence:

$$\sum_{i=1}^n f_i = \sum_{i=1}^n f_{bi} + \sum_{i=1}^n f_{li} + \sum_{i=1}^n f_{ri} \quad (43)$$

As it can be seen by Eq. (38):

$$f_{bi} = - \int_{L_h} M_i h t \, dL - \int_{L_g} M_i j_n t \, dL \quad (44)$$

$$f_{bi} = - \oint_L M_i j_n t \, dL \quad (45)$$

If we consider a component of the load vector:

$$f_{li} = \int_A M_i J t \, dA \quad (46)$$

and of the reaction vector:

$$f_{ri} = - \int_A M_i R_g t \, dA \quad (47)$$

Combining the three previous equations we get:

$$\sum_{i=1}^n f_i = - \oint_L \left(\sum_{i=1}^n M_i \right) j_n t \, dL + \int_A \left(\sum_{i=1}^n M_i \right) J t \, dA - \int_A \left(\sum_{i=1}^n M_i \right) R t \, dA \quad (48)$$

With Eq. (9) we get:

$$\sum_{i=1}^n f_i = 0 \quad (49)$$

The balance principle equals zero because the sum of the individual components of the force vector has the value zero. This conclusion shows that despite of being an approximated method, the balance principle for the body is satisfied.

3.4 Models for microbial metabolism

This section contains the final equations obtained in the formulation for the models. The models pretend to illustrate the consumption of substrates (glucose and xylose), degradation of inhibitors (furfural and HMF) and the influence of the inhibitors on the substrate consumption, without considering microbial growth.

The equations that correspond to all the formulation steps are presented in *APPENDIX A*.

The Fick's law was used to represent the diffusion inside the capsules in all models [17][18].

3.4.1 Model 1: Glucose consumption

The first study case is a simple approach to the glucose consumption in the cell pellet of the capsule. The metabolism of glucose consumption was simulated according to the Monod model [19].

The global balance is represented in Eq. (50):

$$D_g \left(\frac{2}{r} \frac{dC_g}{dr} + \frac{d^2 C_g}{dr^2} \right) - v_{gmax} \frac{C_g}{C_g + K_g} = \frac{dC_g}{dt} \quad (50)$$

Where C_g is the glucose concentration, D_g is the diffusion coefficient for glucose, K_g is the saturation constant for glucose, v_{gmax} is the maximum glucose consumption rate constant, r is the radial position and t the time.

3.4.2 Model 2: Glucose and Xylose co-consumption

Model 2 will include also the Xylose consumption. The two substrates will be considered as competing substrates [20].

The global balances for glucose and xylose are, respectively:

$$D_g \left(\frac{2}{r} \frac{dC_g}{dr} + \frac{d^2 C_g}{dr^2} \right) - v_{gmax} \frac{C_g}{K_g \left(1 + \frac{C_x}{K_{xi}} \right) + C_g} = \frac{dC_g}{dt} \quad (51)$$

$$D_x \left(\frac{2}{r} \frac{dC_x}{dr} + \frac{d^2 C_x}{dr^2} \right) - v_{xmax} \frac{C_x}{K_x \left(1 + \frac{C_g}{K_{gi}} \right) + C_x} = \frac{dC_x}{dt} \quad (52)$$

Where C_x is the xylose concentration, D_x is the diffusion coefficient for xylose, K_x is the saturation constant for xylose, K_{gi} is the inhibition constant of glucose over xylose, K_{xi} is the inhibition constant of xylose over glucose, v_{xmax} is the maximum xylose consumption rate constant.

3.4.3 Model 3: Glucose and inhibitors (furfural and HMF)

The furfural and HMF effects in the glucose consumption were considered as an uncompetitive inhibition [21]. The inhibitors have precedence over glucose consumption and are not affected by its concentration. The combined inhibition was set to 60%, and furfural had a stronger inhibition effect when compared to HMF.

The global balances for glucose, furfural and HMF are next presented by the respective order:

$$D_g \left(\frac{2}{r} \frac{dC_g}{dr} + \frac{d^2 C_g}{dr^2} \right) - v_{gmax} \frac{C_g}{K_g + C_g} \left(\frac{1}{1 + \frac{C_f}{K_{fi}}} \right) \left(\frac{1}{1 + \frac{C_h}{K_{hi}}} \right) = \frac{dC_g}{dt} \quad (53)$$

$$D_f \left(\frac{2}{r} \frac{dC_f}{dr} + \frac{d^2 C_f}{dr^2} \right) - v_{fmax} \frac{C_f}{C_f + K_f} = \frac{dC_f}{dt} \quad (54)$$

$$D_h \left(\frac{2}{r} \frac{dC_h}{dr} + \frac{d^2 C_h}{dr^2} \right) - v_{hmax} \frac{C_h}{C_h + K_h} = \frac{dC_h}{dt} \quad (55)$$

Where C_f is the furfural concentration, C_h is the HMF concentration, D_f is the diffusion coefficient for furfural, D_h is the diffusion coefficient for HMF, K_f is the saturation constant for furfural, K_h is the saturation constant for HMF, K_{fi} is the inhibition constant of furfural, K_{hi} is the inhibition constant of HMF, v_{fmax} is the maximum furfural consumption rate constant and v_{hmax} is the maximum HMF consumption rate constant

3.4.4 Model 4: Glucose and Xylose co-consumption and inhibitors

In this case, all the models are joined together. The equations of the formulation are listed below. Considerations referring to growth and diffusion are the same as those used in the other model [18][20][21].

The global balances for the substrates and inhibitors are enumerated by this order: glucose, xylose, furfural and HMF.

$$D_g \left(\frac{2}{r} \frac{dC_g}{dr} + \frac{d^2 C_g}{dr^2} \right) - v_{gmax} \frac{C_g}{K_g \left(1 + \frac{C_x}{K_{xi}} \right) + C_g} \left(\frac{1}{1 + \frac{C_f}{K_{fi}}} \right) \left(\frac{1}{1 + \frac{C_h}{K_{hi}}} \right) = \frac{dC_g}{dt} \quad (56)$$

$$D_x \left(\frac{2}{r} \frac{dC_x}{dr} + \frac{d^2 C_x}{dr^2} \right) - v_{gmax} \frac{C_x}{K_x \left(1 + \frac{C_g}{K_{gi}} \right) + C_x} \left(\frac{1}{1 + \frac{C_f}{K_{fi}}} \right) \left(\frac{1}{1 + \frac{C_h}{K_{hi}}} \right) = \frac{dC_x}{dt} \quad (57)$$

$$D_f \left(\frac{2}{r} \frac{dC_f}{dr} + \frac{d^2 C_f}{dr^2} \right) - v_{fmax} \frac{C_f}{C_f + K_f} = \frac{dC_f}{dt} \quad (58)$$

$$D_h \left(\frac{2}{r} \frac{dC_h}{dr} + \frac{d^2 C_h}{dr^2} \right) - v_{hmax} \frac{C_h}{C_h + K_h} = \frac{dC_h}{dt} \quad (59)$$

3.4.5 Model 5: Glucose activation effect

The Model 5 was created regarding recent evidences that point towards a maximum xylose uptake for glucose concentration values greater than zero [20]. Equations for the model are presented in *APPENDIX A.5*.

The global balance for glucose is:

$$D_g \left(\frac{2}{r} \frac{dC_g}{dr} + \frac{d^2 C_g}{dr^2} \right) - v_{gmax} \frac{C_g}{K_g \left(1 + \frac{C_x}{K_{xi}} \right) + C_g} = \frac{dC_g}{dt} \quad (60)$$

And for xylose is:

$$D_x \left(\frac{2}{r} \frac{dC_x}{dr} + \frac{d^2 C_x}{dr^2} \right) - R_x = \frac{dC_x}{dt} \quad (61)$$

With:

$$R_x = \begin{cases} v_{xmax1} \frac{C_x}{K_x + C_x} \left(1 + \alpha \frac{C_g}{K_{gi}} \right), & \text{if } 0 \leq C_g < C_{ga} \\ v_{xmax2} \frac{C_x}{K_x \left(1 + \frac{C_g - C_{ga}}{K_{gi}} \right) + C_x}, & \text{if } C_g \geq C_{ga} \end{cases} \quad (62)$$

$$\begin{aligned} v_{xmax1} &= q_{xmax} X \\ v_{xmax2} &= 2 \times q_{xmax} X \end{aligned} \quad (63)$$

Where C_{ga} is the glucose concentration value in which the xylose consumption rate achieves its maximum and α is the value for which the two branches of the equation are equal - at C_{ga} .

3.5 Studies

Two studies were carried in this report and they are explained in the following paragraphs.

3.5.1 Continuous fermentation

The main study in this report is the Continuous fermentation. For models 1 to 5, continuous fermentations were simulated, keeping $C_{J_{bulk}}$ constant.

3.5.2 Validation

As it is very difficult to obtain data for profile concentrations inside the capsules, in order to validate the results obtained in the Continuous fermentation study, batch fermentations were simulated and results compared to published data of glucose concentration in the bulk solution. To achieve that, model 1 and model 3 without HMF methodology was used.

This study was performed for non-growing cell case and the effect of cell growth inside the capsule was analyzed too. For the non-growing cell case the models will be called NG, for the growing system three different scenarios were tested and named $G1$, $G2$ and $G3$.

3.6 Assumptions

In the next points, the general assumptions for the formulation of the models are enumerated:

- i. the cells are only distributed in half of the sphere – cell pellet;
- ii. the degradation of sugars and inhibitors occur only inside the cell pellet;
- iii. there are no external mass transfer resistances;
- iv. the membrane of the capsule does not represent an important mass transfer limitation (value of the diffusion in the membrane is 90 % of the diffusion of the substances in the hydrolysate).

3.7 Kinetic and diffusion parameters – bibliographic revision

The search for published data values for kinetic and diffusion parameters is included in this section of the report. This search was done to support the choice of values used in the formulation of models in COMSOL.

In *Table 2* are represented data values for some diffusion coefficients of glucose, xylose, furfural and HMF and *Table 3* shows the kinetic values.

Table 2. Diffusion coefficients for the fermentation substrates and inhibitors

$\frac{D_g \times 10^6}{cm^2/s}$	$\frac{D_x \times 10^6}{cm^2/s}$	$\frac{D_f \times 10^6}{cm^2/s}$	$\frac{D_h \times 10^6}{cm^2/s}$	Conditions	Ref.
8.9	9.9	-	-	Diffusion experiments performed at 30°C, in water	[22]
8.1	9.2			Diffusion experiments performed in inoculated agar gel layer	[22]
6.8	-	-	-	Fermentation by <i>S.cerevisiae</i> in flocs (Ca-alginate 2%)	[23]
5.5				Fermentation by <i>S.cerevisiae</i> in flocs (Ca-alginate 2% with yeast 20% w/v)	[23]
6.76	7.69	11.2	10.6	Proprieties in hydrolyzate	[24]

*Note: D_{gw} , diffusion coefficient for glucose; D_x , diffusion coefficient for xylose; D_f , diffusion coefficient for furfural; D_h , diffusion coefficient for HMF.

Table 3. Kinetic parameters for glucose, xylose, furfural and HMF consumption by *Saccharomyces cerevisiae* – bibliography review

Conditions	Ref.	$\frac{Y_{E/g}}{g/g}$	$\frac{r_E}{g/(L h)}$	$\frac{q_{Emax}}{g/(g h)}$	$\frac{q_{gmax}}{mmol/(g h)}$	$\frac{q_{xmax}}{mmol/(g h)}$	$\frac{Y_{X/g}}{g/g}$	$\frac{Y_{X/x}}{g/g}$	$\frac{\mu}{h^{-1}}$	$\frac{K_g}{mM}$	$\frac{K_x}{mM}$	$\frac{K_f}{g/L}$	$\frac{q_{fmax}}{g/(g h)}$	$\frac{q_{hmax}}{g/(g h)}$
Anaerobic continuous fermentation by encapsulated <i>S.cerevisiae</i> (D=0.2 h ⁻¹) (on glucose)	[25]	0.40 ± 0.03	1.64	0.26 ^a	-	-	-	-	-	-	-	-	-	-
Anaerobic continuous fermentation by encapsulated <i>S.cerevisiae</i> (D=0.2 h ⁻¹) (on dilute-acid hydrolysate)	[25]	0.45 ± 0.01	2.053	0.16 ^b	-	-	-	-	-	-	-	-	-	-
Anaerobic batch fermentation by encapsulated <i>S.cerevisiae</i> (batch 1) (synthetic media with 5 g/L of furfural)	[26]	0.41	1.63	-	-	-	-	-	-	-	-	-	-	-
Nongrowing, anaerobic, compressed <i>S.cerevisiae</i>	[27]	-	-	-	8.64 ^c	-	-	-	-	-	-	-	-	-
CSTR with glucose, cyanide and a suspension of starved yeast cells flow	[28]	-	-	-	-	-	-	-	-	1.7	-	-	-	-
Anaerobic batch fermentation by encapsulated <i>S.cerevisiae</i> (20 g/L glucose)	[19]	0.66	-	1.27	-	-	0.49	-	-	2.16 ^c	-	-	-	-
Anaerobic batch fermentation by free <i>S.cerevisiae</i> RBW 218 (100 g/L glucose and 25g/L xylose)	[29]	0.38 ± 0.01	-	-	7.3 ± 0.3	32.0 ± 2.0	0.084 ± 0.001	-	0.22 ± 0.00	5.7 ± 1.0	99 ± 16	-	-	-
Anaerobic continuous fermentation by free <i>S.cerevisiae</i> (D=0.315 h ⁻¹) (on synthetic medium with addition of furfural 2.0 g/L)	[30]	0.439	-	-	-	-	0.12	-	-	-	-	-	0.15	-
Anaerobic continuous fermentation by free <i>S.cerevisiae</i> (D=0.275 h ⁻¹) (on synthetic medium with pulse of furfural 4.0g/L)	[30]	-	-	-	-	-	-	-	0.198 ± 0.051	-	-	1.22 ± 0.52	0.62 ± 0.06	-
Anaerobic batch fermentation by free <i>S.cerevisiae</i> (on synthetic medium with glucose 50g/L and pulse of furfural 2.0g/L and HMF of 2.0g/L)	[31]	0.42 ± 0.02	-	0.45 ± 0.11	-	-	0.054 ± 0.006	-	0.01 ± 0.01	-	-	-	-	0.036 ± 0.011
Anaerobic batch fermentation by free <i>S.cerevisiae</i> (on synthetic medium with glucose 50g/L and pulse of furfural 4.0g/L)	[31]	0.4	-	0.7	-	-	0.067	-	0.05	-	-	-	-	-
Anaerobic batch fermentation by free <i>S.cerevisiae</i> (on synthetic medium with glucose 50g/L and pulse of HMF of 4.0g/L)	[31]	0.42 ± 0.01	-	0.95 ± 0.05	-	-	0.059 ± 0.001	-	0.13 ± 0.00	-	-	-	-	0.14 ± 0.03
Anaerobic culture of wild-type <i>S. cerevisiae</i> CEN.PK113-7D and the XylA-expressing strain RWB 202 (20 g/L of glucose and 10g/L of xylose)	[32]	-	-	-	0.73±0.00	-	-	-	-	-	-	-	-	-
Anaerobic batch fermentation by free <i>Saccharomyces</i> yeasts 1400 (glucose and xylose)	[33]	0.47	-	-	-	-	0.115	0.162	-	3.14 ^c	22.65 ^c	-	-	-

*Note: a, per glucose; b, per glucose, mannose and galactose; c, calculated from the reference. $Y_{E/g}$, ethanol yield on glucose; r_E , volumetric ethanol production rate; q_{Emax} , maximum specific productivity of ethanol; q_{gmax} , maximum specific productivity of glucose; q_{xmax} , maximum specific productivity of xylose; $Y_{X/g}$, biomass yield on glucose; $Y_{X/x}$, biomass yield on xylose; μ , specific growth rate; K_g , monod constant for glucose; K_x , monod constant for xylose; K_f , monod constant for furfural; q_{fmax} , maximum specific furfural conversion rate; q_{hmax} , maximum specific furfural conversion rate.

3.8 Fermentation parameters for the models

Table 4 shows the values used for models 1 to 5 in the Continuous fermentation study. The membrane, cell pellet and liquid core diffusions are, respectively, 90%, 100% and 50% of the diffusion of the substrate in hydrolysates.

Table 4. Kinetic and diffusion values for the models 1 to 5

Designation	Symbol	Value	Unit
Biomass concentration inside the capsule	X	133	g/L
Glucose concentration outside the capsule	C_{gout}	40	g/L
Glucose concentration for glucose activation	C_{ga}	0.4	g/L
Maximum specific glucose consumption rate constant	q_{gmax}	0.01	$mol/(g\ h)$
Saturation constant for glucose	K_g	1.7	mol/m^3
Inhibition constant of glucose	K_{gi}	1.7	mol/m^3
Diffusion coefficient of glucose in the membrane	D_{gm}	6.08×10^{-10}	m^2/s
Diffusion coefficient of glucose in the cell pellet	D_{gc}	3.38×10^{-10}	m^2/s
Diffusion coefficient of glucose in the liquid core	D_{gw}	6.76×10^{-10}	m^2/s
Xylose concentration outside the capsule	C_{xout}	20	g/L
Maximum specific xylose consumption rate constant	q_{xmax}	0.001	$mol/(g\ h)$
Saturation constant for xylose	K_x	20	mol/m^3
Inhibition constant of xylose	K_{xi}	20	mol/m^3
Diffusion coefficient of xylose in the membrane	D_{xm}	6.92×10^{-10}	m^2/s
Diffusion coefficient of xylose in the cell pellet	D_{xc}	3.85×10^{-10}	m^2/s
Diffusion coefficient of xylose in the liquid core	D_{xw}	7.69×10^{-10}	m^2/s
Furfural concentration outside the capsule	C_{fout}	2	g/L
Maximum specific furfural consumption rate constant	q_{fmax}	0.006	$mol/(g\ h)$
Saturation constant for furfural	K_f	13	mol/m^3
Inhibition constant of furfural	K_{fi}	20.8	mol/m^3
Diffusion coefficient of furfural in the membrane	D_{fm}	1.01×10^{-9}	m^2/s
Diffusion coefficient of furfural in the cell pellet	D_{fc}	5.60×10^{-10}	m^2/s
Diffusion coefficient of furfural in the liquid core	D_{fw}	1.12×10^{-9}	m^2/s
HMF concentration outside the capsule	C_{hout}	2	g/L
Maximum specific HMF consumption rate constant	q_{hmax}	0.001	$mol/(g\ h)$
Saturation constant for HMF	K_h	30	mol/m^3
Inhibition constant of HMF	K_{hi}	63.4	mol/m^3
Diffusion coefficient of HMF in the membrane	D_{hm}	9.54×10^{-10}	m^2/s
Diffusion coefficient of HMF in the cell pellet	D_{hc}	5.30×10^{-10}	m^2/s
Diffusion coefficient of HMF in the liquid core	D_{hw}	1.06×10^{-9}	m^2/s
Correction parameter for glucose activation effect	α	0.77	-

3.9 COMSOL Multiphysics

The COMSOL Multiphysics is a modeling program with the ability to solve problems related to different fields.

To solve the problems, COMSOL follows the Finite Element Method and computational meshing using numerical solvers [34].

The problems are based on partial differential equations and by using its applications it provides various kinds of analysis such as: stationary and time-dependent analysis, linear and nonlinear analysis [34].

3.10 Simulation steps in COMSOL

Figure 5 shows the different steps taken in COMSOL.

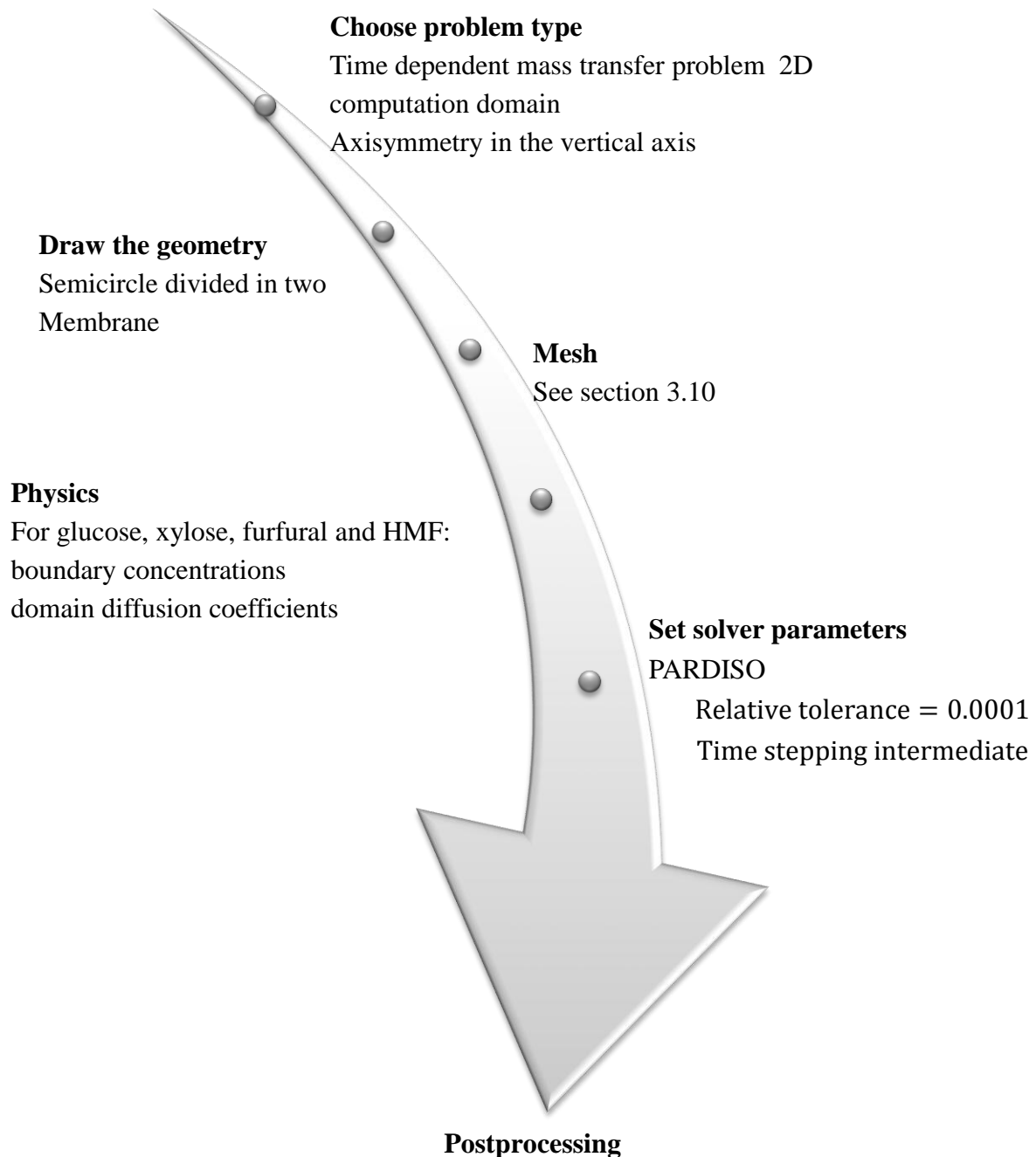


Figure 5. Steps of the formulation process in COMSOL.

3.11 COMSOL scheme for Continuous fermentation

The geometry in 3D is a sphere with a 2 mm radius and 0.17 mm of membrane thickness. The core of the sphere is divided in two: the liquid core and the cell pellet.

Figure 6 shows the 2D representations in Comsol of half of the capsule (symmetry axis, in the vertical axis, $2\pi r$) for the Continuous fermentation cases.

The concentrations in the bulk outside the capsule are maintained constant.

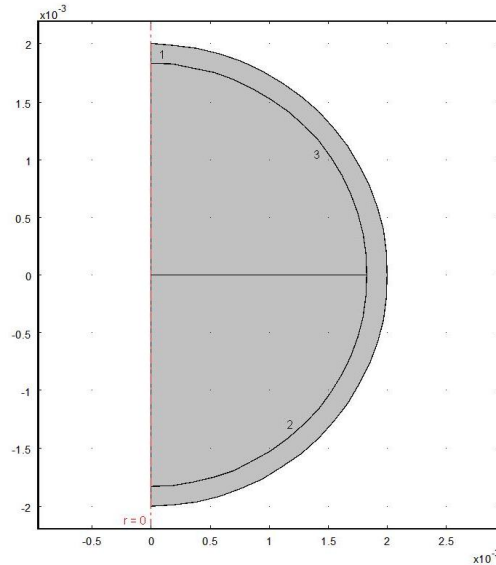


Figure 6. 2D geometry in COMSOL simulating the Capsule structure: 1- Membrane; 2- Cell pellet and 3- Liquid core.

3.12 COMSOL scheme for Validation

In Validation, schemes try to simulate batch cultivation. The bulk concentrations of substrates decrease according to consumption and diffusion rates.

The obtained scheme obtained resulted from was based in the definition of an average volume surrounding the capsule in which the substrates are perfectly mixed, *APPENDIX C*.

The diffusion coefficient in the medium volume was set to $1000 \times D_{sw}$ with the purpose to avoid concentration gradients outside the sphere, which simulates the perfect stirred mixture.

3.12.1 NG

Figure 7 presents the scheme used for the simulation of model 1 and model 3 (without HMF) with no growth in the validation.

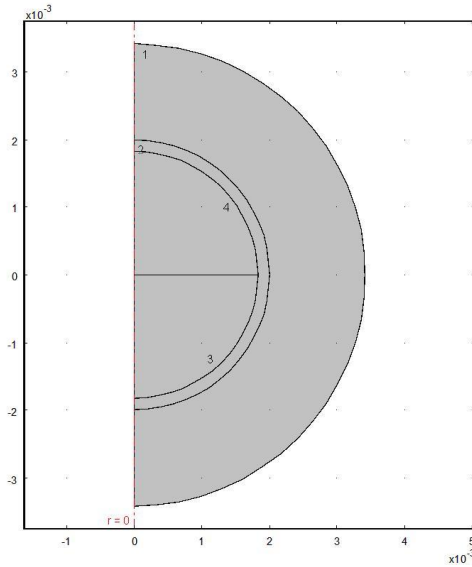


Figure 7. 2D COMSOL geometry for the batch simulation for model 1 and 3 (without HMF): 1- Average medium volume; 2- Membrane; 3- Cell pellet and 4- Liquid core.

3.12.2 G1

Study G1 has the same geometry as the NG. Supposedly, the cells were initially concentrated in half of the sphere volume, *Figure 8*.

The growth was simulated by changing diffusion conditions inside the cell pellet and with the increase of X . It was considered that the diffusion coefficient decreases while the cells grow, according to the *Appendix D*. The cells will grow according to *Appendix E*.

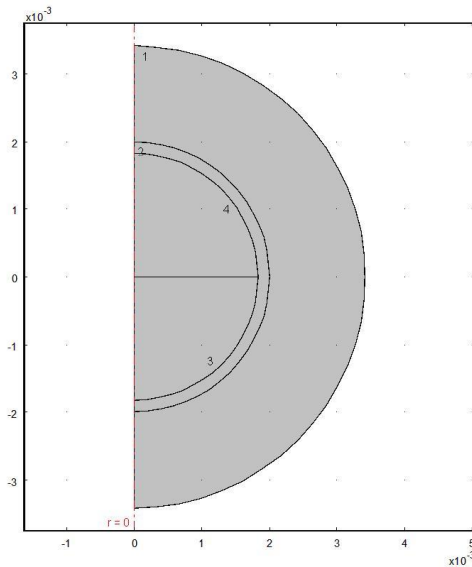


Figure 8. 2D Geometry in COMSOL. Case of the growth inside half sphere. 1- Average medium volume; 2- Membrane; 3- Cell pellet and 4-Liquid core.

3.12.3 G2

The concept in study G2 is the same of G1, but in this one, the cells are distributed in the whole interior volume of the sphere, as it can be seen in *Figure 9*. See also *Appendix D* and *Appendix E* regarding the variation of the diffusion coefficients and biomass concentration.

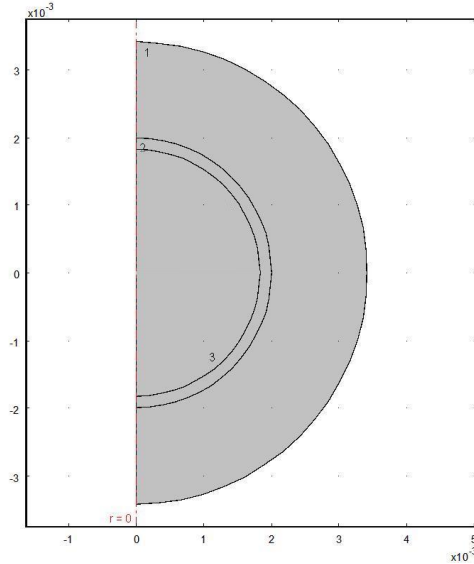


Figure 9. 2D Geometry for the cell growth simulation for the entire capsule filled with cells. 1- Average medium volume; 2- Membrane and 3- Cell pellet.

3.12.4 G3

At first the cells were concentrated in a small volume of the sphere. The cell growth was defined by a constant increase of the volume occupied by the cells, keeping the concentration of the cells constant in that volume. The increase of the volume was simulated by the movement of the cell pellet boundary with the liquid core, *Figure 10*. A boundary movement velocity was calculated according to the *APPENDIX F*.

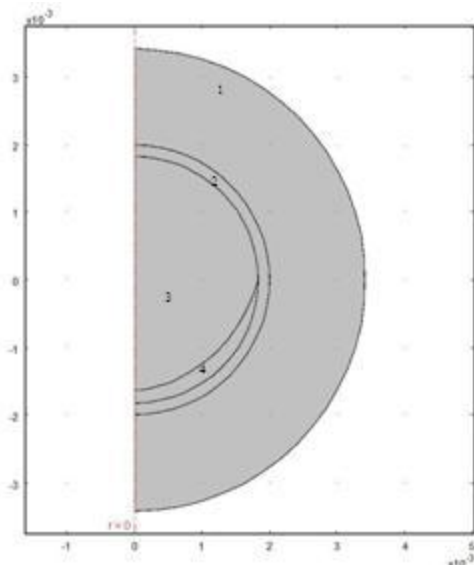


Figure 10. 2D Geometry in COMSOL - moving boundary. 1- Average medium volume; 2- Membrane; 3- Liquid core and 4- Cell pellet.

3.13 Mesh in COMSOL

Creating a mesh in COMSOL comprises various steps and choices. The main ones are presented in the *Figure 11*.

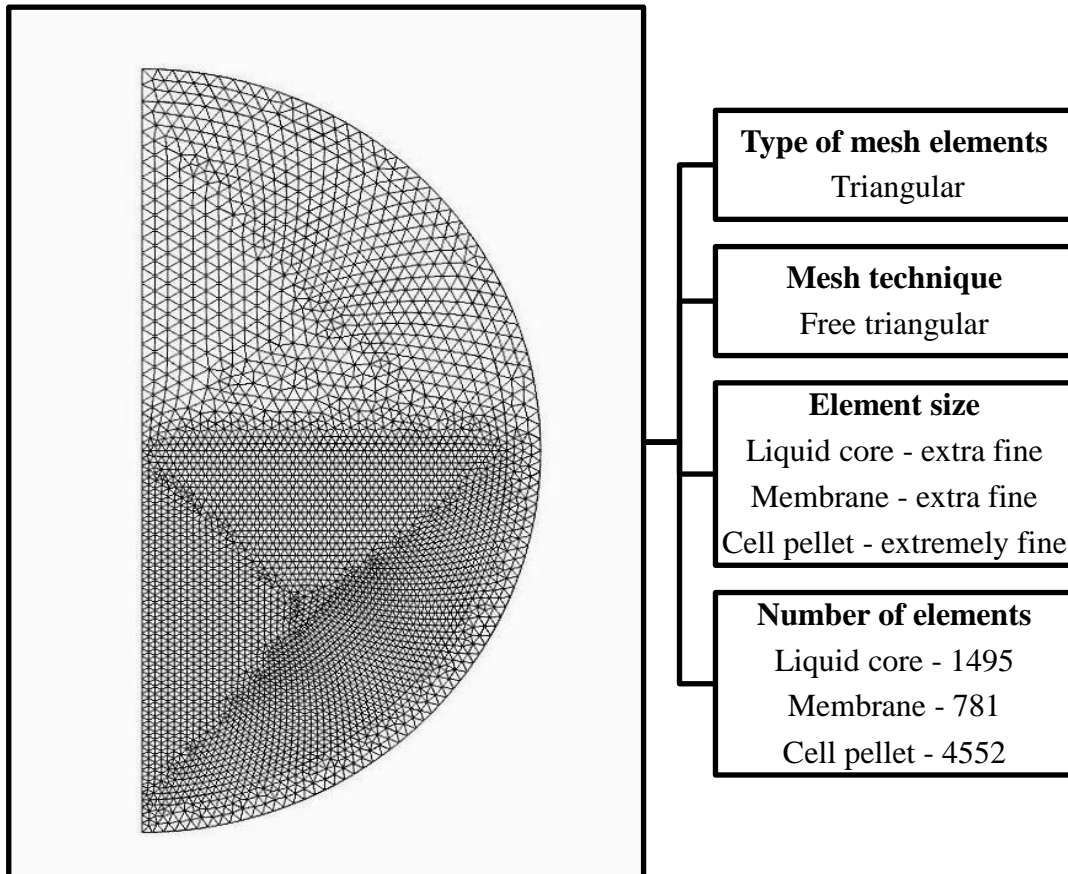


Figure 11. Options taken in the process of Mesh creation in COMSOL.

4. ANALYSIS AND DISCUSSION OF RESULTS

In this section are presented the results and their respective discussion. They were enumerated by models, and in each model were obtained concentration profiles and post-processing plots and parameters that the authors find to be relevant.

The substrates and inhibitors uptake rates were calculated by computing the Surface Integration over the cell pellet and by multiplying the results by the respective area.

Profile concentrations were obtained for the time considered as stationary state. The stationary state was defined by the first “Truth” in the logic test made in Excel for the uptake values. The logic test verified all the values and gave “Truth” for those whose values have less than 0.1 % difference with the uptake value in the infinite (86400 s).

For each model, an efficiency factor was calculated dividing the uptake rates in stationary state for that model, and for the same model with maximum diffusion coefficients (D_{sw}) in all domains.

The color scales were chosen with the aim to clearly illustrate concentration profiles inside the capsule, and because of that scales are different for all components.

4.1 Continuous fermentation: Model 1 to 4

4.1.1 Concentration profiles

Figure 12 shows the steady state concentration profile of the fermentation media components for model 1 to 4. The values for the presented consumption rates are per m^3 of cell pellet.

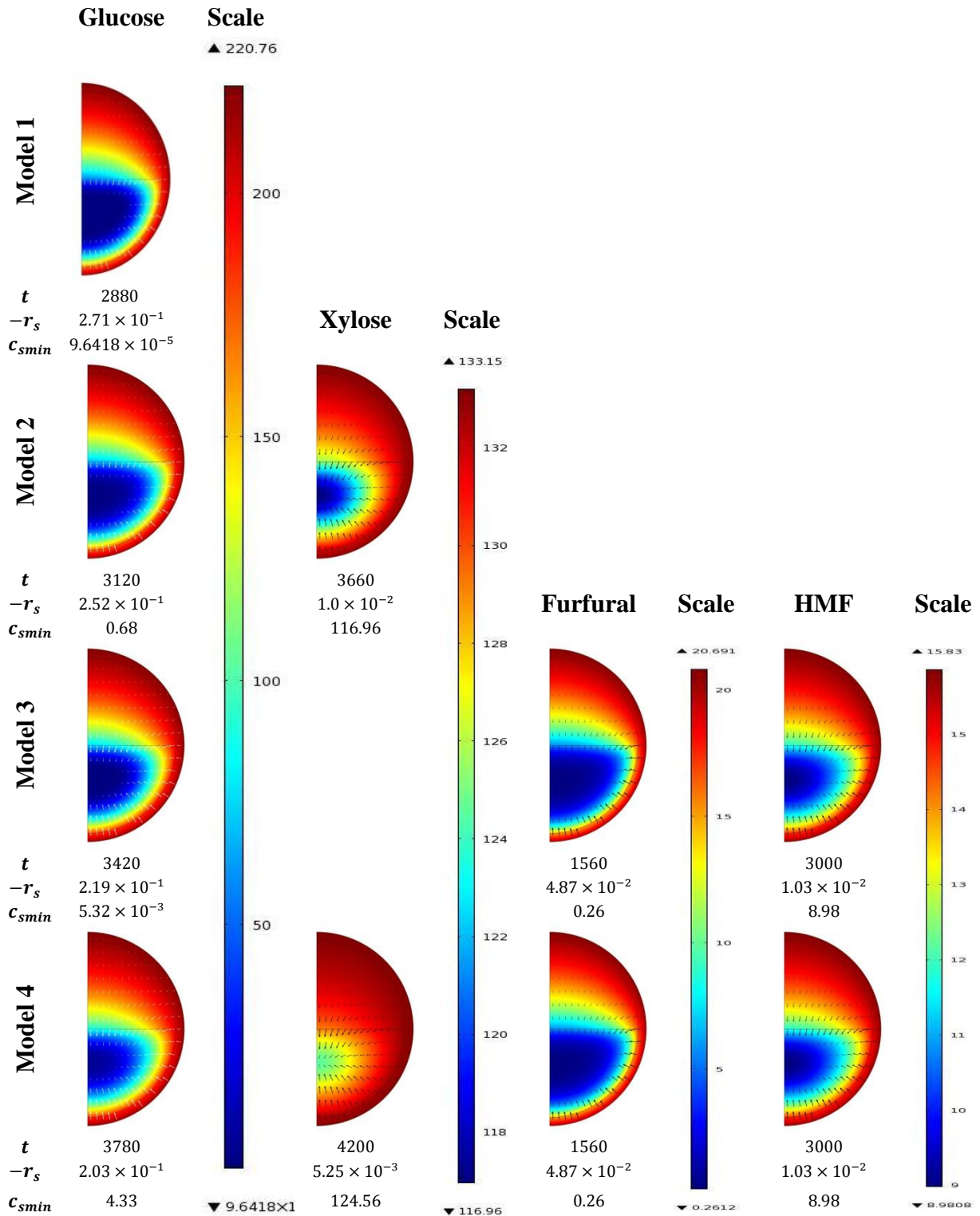


Figure 12 Profile concentrations of substrates and inhibitors for models 1 to 4. Time, t /s; consumption rate, r_s /($mol/(m^3s)$) and minimum concentration inside the capsule $c_{smín}$ /(mol/m^3).

In all the models the stationary state was achieved before the end of the second hour of fermentation.

Through the observation of *Figure 12* it can be concluded that glucose consumption is inhibited by xylose, furfural and HMF in the encapsulated system. The strongest inhibition is caused by furfural and HMF, and that can be based on the higher value for the time when the stationary state was achieved, and in the fact that glucose is not all consumed in the presence of inhibitors.

The reduction of the consumption rate of glucose from model 1 to model 4 was 25.1 %.

Xylose consumption is also highly inhibited by glucose, furfural and HMF. In model 2, when the stationary state is achieved, the cells are only able to convert approximately 12.2 % of the xylose present in the bulk. For model 4 the conversion decreased to approximately 6.5 %.

Furfural has a higher consumption when compared to HMF, approximately 56.7 % of HMF is not converted.

Furfural and HMF have the same profile concentration for model 3 and model 4. This was expected because the formulation had already predicted that the inhibitors had precedence over xylose and glucose consumption.

4.1.2 Dimensionless glucose plots

Dimensionless plots represent a more generalized type of result. This means that they can be used to understand and obtain information about other systems with similar conditions. It is also an important tool that helps to describe and understand the system concisely.

Figure 13 symbolizes the cut line 2D obtained in COMSOL. This data set was used to obtain the values along the radius coordinate in the cell pellet.

Figure 14 shows the correspondent solutions achieved along the cut line length, for glucose concentration in models 1 to 4. *Figure 15* shows the same for all the components in model 4.

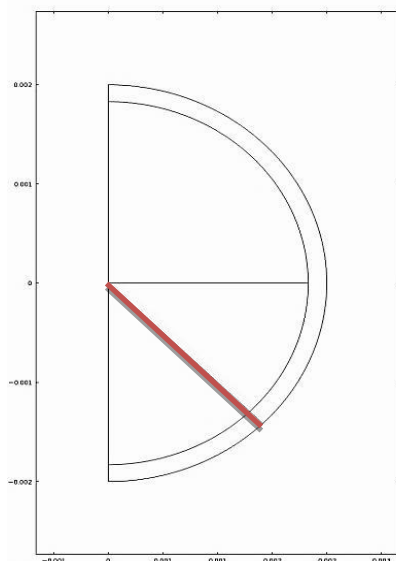


Figure 13. Cut line 2D in COMSOL.

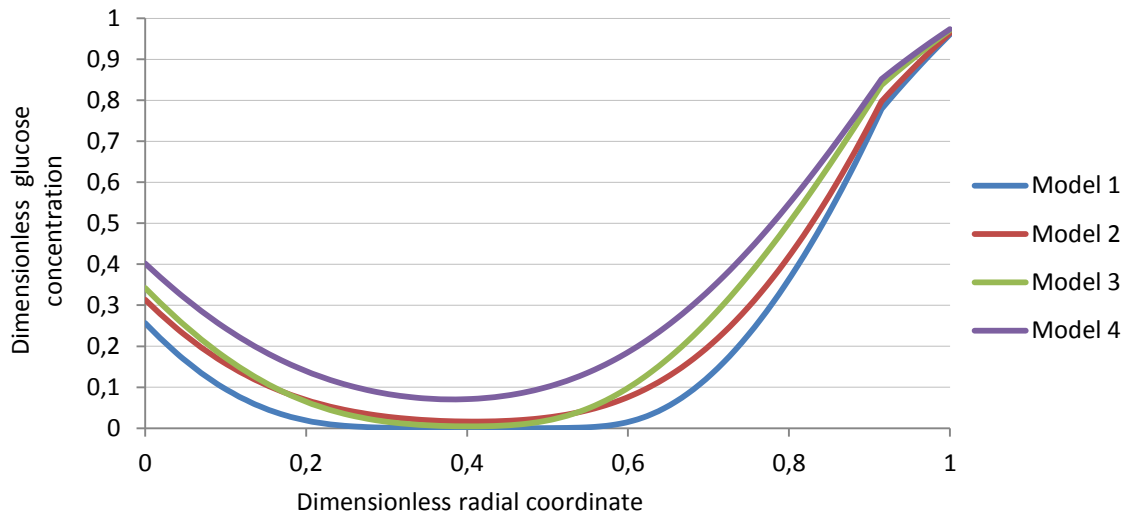


Figure 14. Profiles of dimensionless glucose concentration in the dimensionless radial coordinate.

First of all, it can be observed that the concentration of glucose decreases from the bulk to close to the middle of the cell pellet, where it increases as it goes in the direction of the center of the sphere. Glucose enters in the membrane and crosses it. Then it starts to diffuse into the cell pellet and starts to be consumed at the same time.

The low concentration values for model 1, 2, 3 in the dimensionless capsule radial coordinate of 0.4 reveals that the reactions are limited by the diffusion. In model 4 the reaction is limited kinetically by the presence of xylose, furfural and HMF.

As it crosses the middle of the cell pellet, the concentration rises because of the diffusion of glucose from the liquid core of the capsule. The concentration in the center of the sphere is less than half of the bulk which reveals that the diffusion rate is not high enough to compensate the consumption reaction.

From the observation of *Figure 15*, it can be pointed out that furfural has the highest consumption followed by glucose.

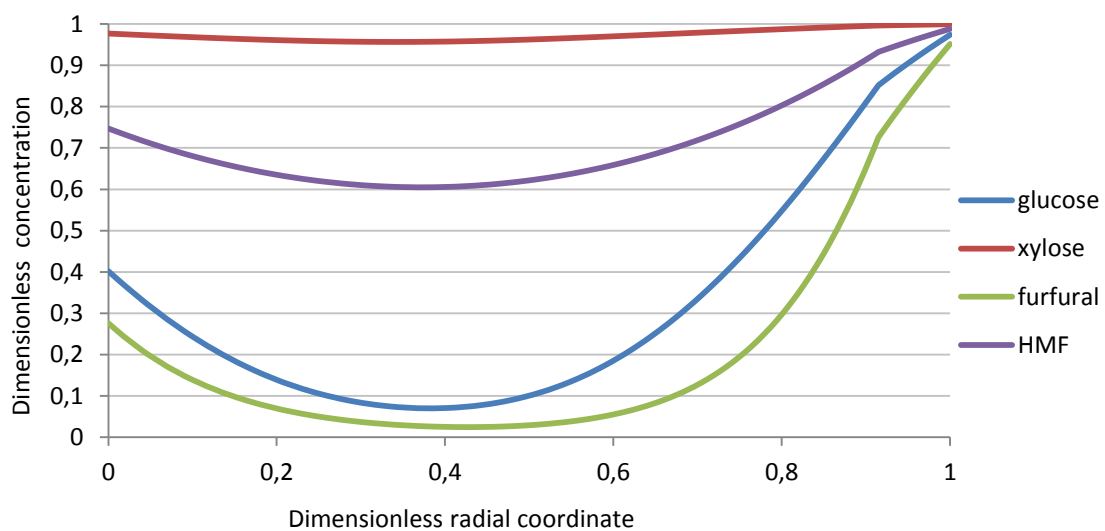


Figure 15. Dimensionless concentrations of substrates and inhibitors along the dimensionless radial coordinate for model 4.

Xylose is almost not consumed, inhibited by glucose, furfural and HMF. Xylose is only consumed in the capsule zone where glucose, furfural and HMF are in smaller concentrations (inhibition effect is smaller).

4.1.3 Consumption reaction plots

Figure 16 and Figure 17 are graphic representations of the consumption rates with time. In Figure 16 it can be seen the consumption reactions in model 4. In Figure 17 it can be visualized the difference between the consumption rates for xylose in model 2 and 4.

It can be concluded that, relatively to xylose consumption in model 2 and 4, the difference between the curves are due to the inhibition effect caused by furfural and HMF.

Now, focusing on the xylose uptake rate values for model 4 in Figure 17, it can be perceived that the uptake grows, and decreases after achieving a maximum value.

The maximum value ($6.48 \times 10^{-3} \text{ mol}/(\text{m}^3 \text{ s})$) corresponds to the time (660 s). This

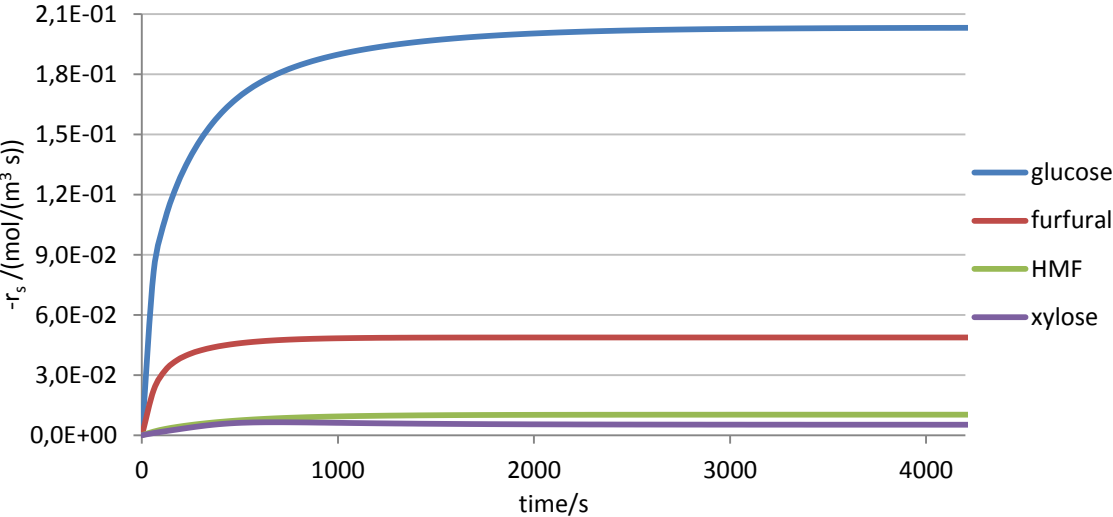


Figure 17. Uptake kinetics for glucose, xylose, furfural and HMF in model 4.

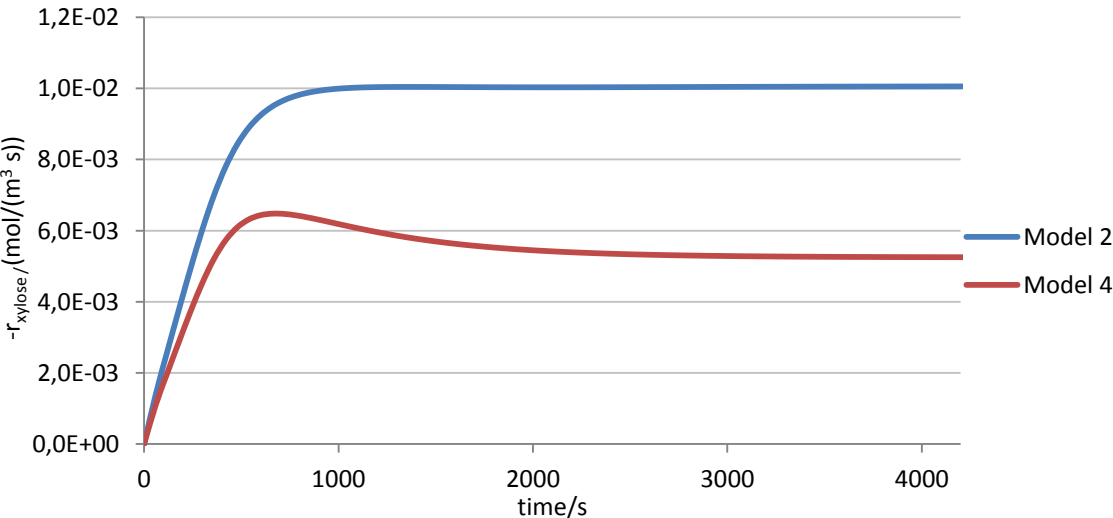


Figure 16. Xylose consumption rate through the time for model 2 and for model 4.

situation could be interesting to improve xylose consumption.

In *Figure 18*, glucose and xylose concentration profiles for that time are represented.

Xylose has a higher diffusion coefficient which means that it arrives first (*figure 18.a* and *Figure 18.b*) than glucose (inhibited by furfural and HMF and slowed by the diffusion) at the center of the sphere.

It can be seen in *Figure 18.c* and *Figure 18.d* that there is an area close to the center of the cell pellet where the reaction of xylose has its maximum. This area corresponds to the zone

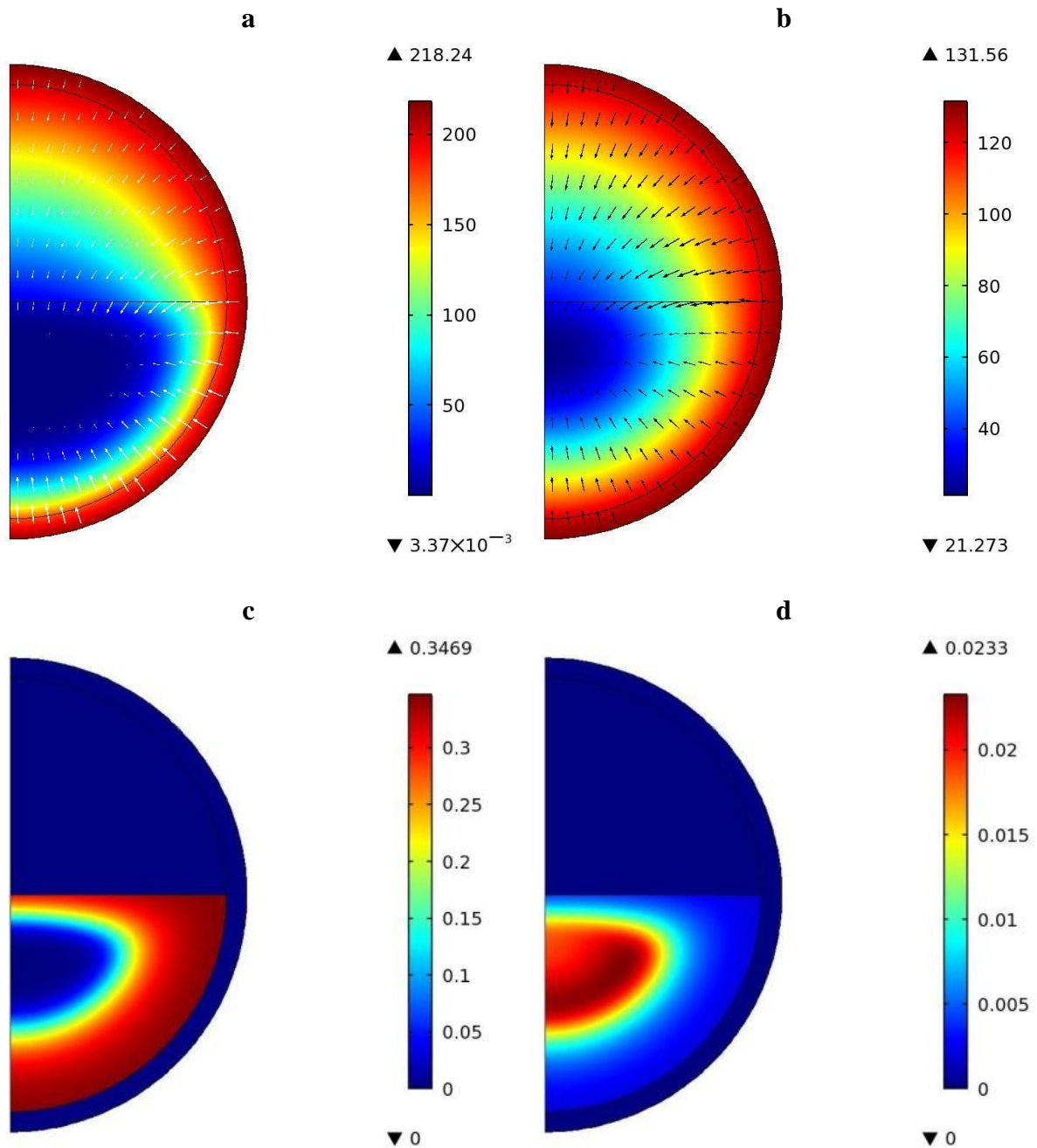


Figure 18. a. Glucose concentration profile (mol/m^3); b. Xylose concentration profile (mol/m^3); c. Glucose consumption rate profile ($\text{mol}/(\text{m}^3 \text{ s})$); d. Xylose consumption rate profile ($\text{mol}/(\text{m}^3 \text{ s})$), for time = 660 s in model 4.

where the reaction of glucose is very low because of consumption and diffusion-limited transport of glucose into the capsule.

4.1.4 Efficiency factor

As was said before, the efficiency factor is the ratio between the consumption rate for each model and the consumption rate in a so-called maximum diffusion model, in which the diffusion coefficient in all the domains was $1000 \times D_{sw}$. This model is intended to represent a system of free cells.

The mere observation of this factor can tell if the encapsulation of the cells is favorable ($\eta > 1$) or not ($\eta < 1$) to the consumption of the substrates and inhibitors.

Table 5 shows the values achieved for this factor. The values obtained suggested that there is no benefit for glucose consumption to the encapsulated cells when it is not in presence of furfural and HMF. Yet, when inhibitors are added, the encapsulation becomes beneficial.

For xylose, the encapsulation is always favorable when compared with the maximum diffusion model. While reducing the concentration of glucose inside the capsules because of the mass transfer resistance, the cells can now consume xylose.

As the model just considers the consumption reaction with no harmful for cells (cellular death) for furfural and HMF, it was expected a value lower than one. This means that in the encapsulated case, higher diffusion limitations occurs when compared to the free cells case, resulting in lower consumption reactions for the inhibitors.

Table 5. Efficiency factor for glucose, xylose, furfural and HMF in the models

Model	Component	$\frac{-r_{smax.dif}}{mol/(m^3s)}$	$\frac{-r_s}{mol/(m^3s)}$	η
1	Glucose	3.66×10^{-1}	2.71×10^{-1}	0.74
2	Glucose	3.48×10^{-1}	2.52×10^{-1}	0.72
	Xylose	1.83×10^{-3}	1.00×10^{-2}	5.50
3	Glucose	1.52×10^{-1}	2.19×10^{-1}	1.44
	Furfural	1.33×10^{-1}	4.87×10^{-2}	0.37
	HMF	1.27×10^{-2}	1.03×10^{-2}	0.81
4	Glucose	1.45×10^{-1}	2.03×10^{-1}	1.40
	Xylose	7.46×10^{-4}	5.25×10^{-3}	7.04
	Furfural	1.33×10^{-1}	4.87×10^{-2}	0.37
	HMF	1.27×10^{-2}	1.03×10^{-2}	0.81

*Note: $-r_{smax.dif}$, reaction rate in the maximum diffusion case; $-r_s$, reaction rate at the normal conditions; η , efficiency factor.

4.2 Continuous fermentation: Model 5

In APPENDIX A.5, the formulation for model 5 implies that xylose consumption rate achieves its maximum at $C_g > 0$.

4.2.1 Concentration and reaction profiles

In Figure 19, the concentration and reaction profiles for glucose and xylose in the end of the study time are presented.

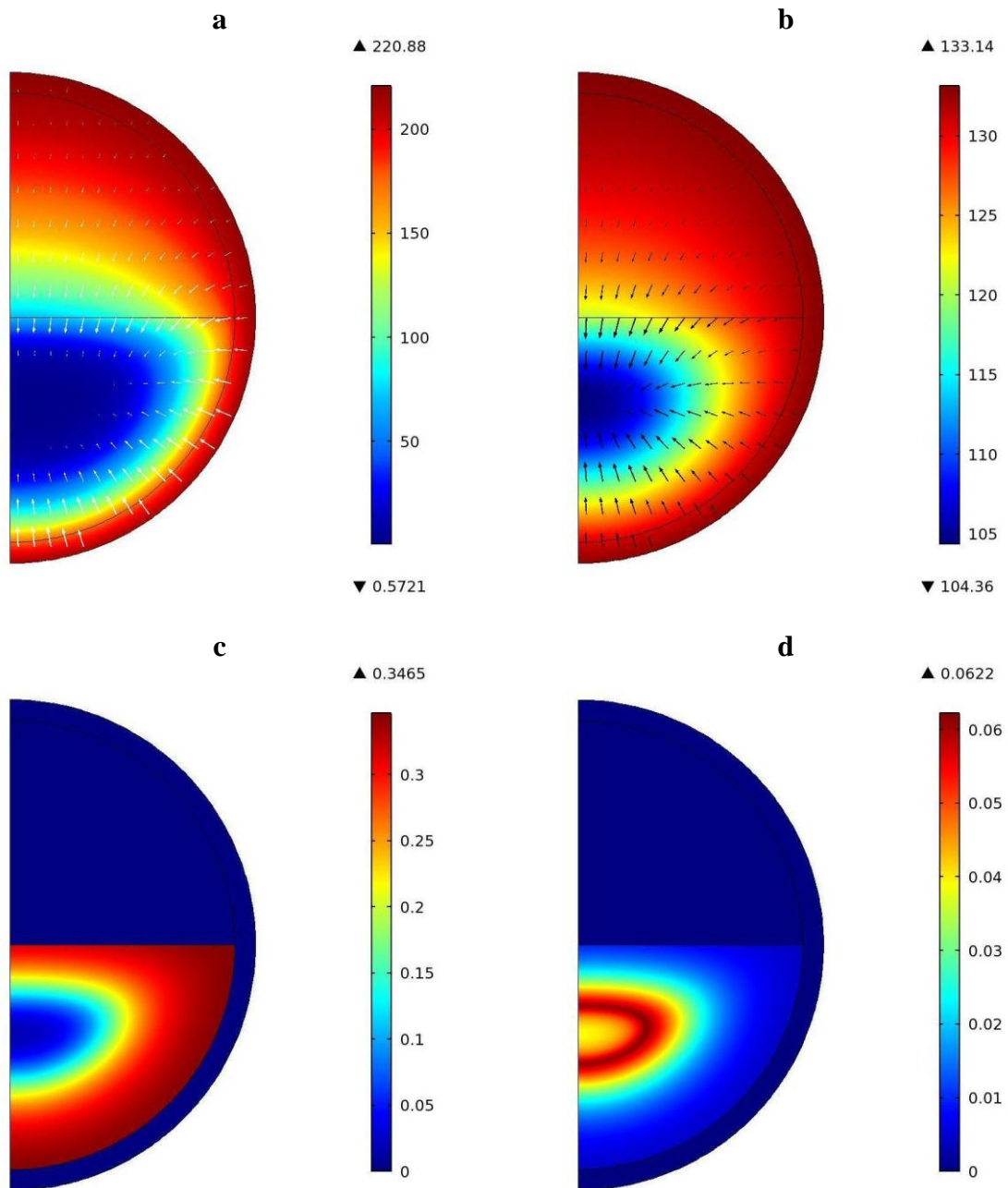


Figure 19. a. Glucose concentration profile (mol/m³); b. Xylose concentration profile (mol/m³); c. Glucose consumption rate profile (mol/(m³ s)); d. Xylose consumption rate profile (mol/(m³ s)), for time = 86400 s in model 5.

It can be observed that the maximum value for the xylose consumption rate happens, not in the center of the sphere, where the glucose concentration is close to zero, but in a zone where there is still some glucose and the value for the reaction is $6.22 \times 10^{-2} \text{ mol}/(\text{m}^3 \text{ s})$.

4.2.2 Consumption reaction plots

A cut line was designed in COMSOL, *Figure 20*, in order to obtain the plot for xylose consumption reaction changing with glucose concentration along the cutline, *Figure 21*.

The cut line was drawn with the objective to cross only once the region where the xylose consumption rate has its maximum value, and for that *Figure 19.b* was used as a guideline.

It can be seen that the reaction achieves its maximum for a value of $C_g = 0.4 \text{ g/L}$.

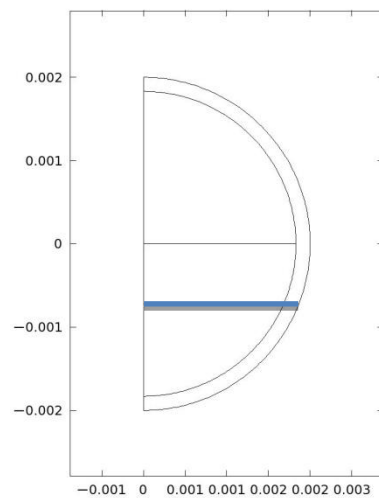


Figure 21. Cut line 2D in COMSOL for glucose activation effect plot (blue line).

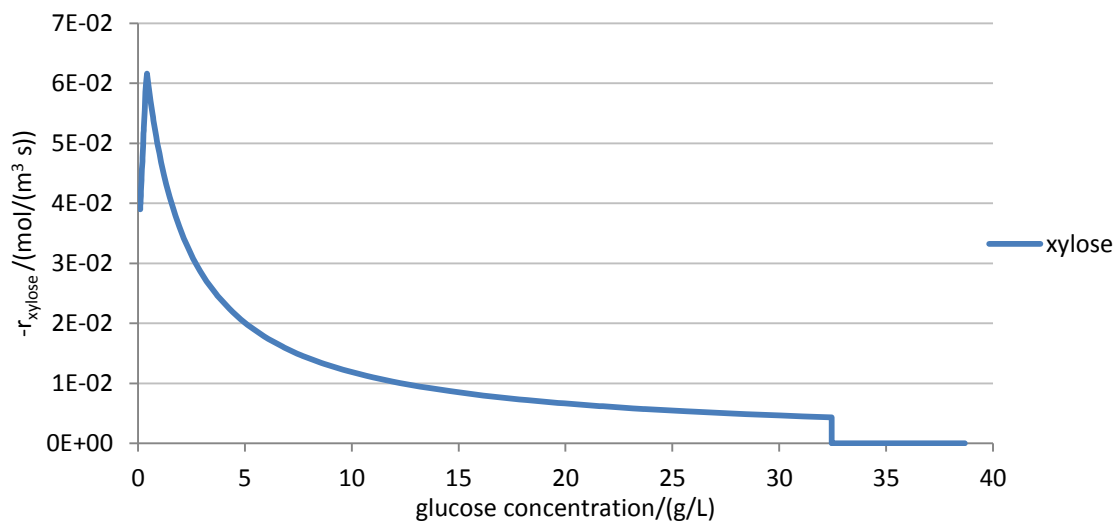


Figure 20. Xylose consumption rate as a function of glucose concentration along the cut line.

4.3 Validation

Due to the difficulty to obtain experimental data for concentrations inside the sphere, batch simulations were performed in order to make possible the comparison between the bulk concentrations and experimental data. For the comparison, data values from the work of Talebnia et al [35] were used.

The three ways of describing growth (G1, G2 and G3) were used in order to test the influence of the cell growth in the fermentations, but also to compare with the no growth case (NG).

G1 assumed that cells grow confined to half of the sphere and that the diffusion coefficients change with the growth according to *APPENDIX D*. G2 considered that the cells were distributed uniformly inside the entire capsule volume. G3 assumed that the cells grow from one point, attached to the inner wall of the membrane [26] and the diffusion coefficients change with the growth according to *APPENDIX D*. None of these descriptions of the growth is really reasonable, but were chosen because they were possible to implement in COMSOL and showed how various growth modes would affect the concentration profiles.

4.3.1 Batch cultivation of glucose

Conditions were defined for the batch fermentation to match the conditions of the fermentations done in [35]. The concentration of glucose was set to 50 g/L , the initial concentration of biomass was 16.22 g/L in G2, which corresponds to a concentration of 32.44 g/L in the cell pellet of the model G1.

All the other parameters were kept constant except the value for q_{max} which was tested for two values, the value used in the Continuous fermentation studies (0.01 mol/(g h)) and another one obtained from an approximation to the published data values, $q_{max.a} = 0.02 \text{ mol/(g h)}$ [35].

The results from the first one are presented as NG, G1, G2 and G3, and the results with the adapted parameter, $q_{max.a}$, as NG.a, G1.a, G2.a, and G3.a.

The results from this simulation and the experimental data from Farid Talebnia [35] are plotted in the *Figure 22*.

From its observation, it can be concluded that the curves that fit better the experimental data are the curves of the G1.a and G3.a (with the changed q_{max}) and from this two curves, it is very difficult to say which one has the higher fit.

In all models, the change of q_{max} caused a significant improvement in the approximation to the experimental data meaning that in the experimental setup, the reaction of consumption is slower than the models that were created in this project.

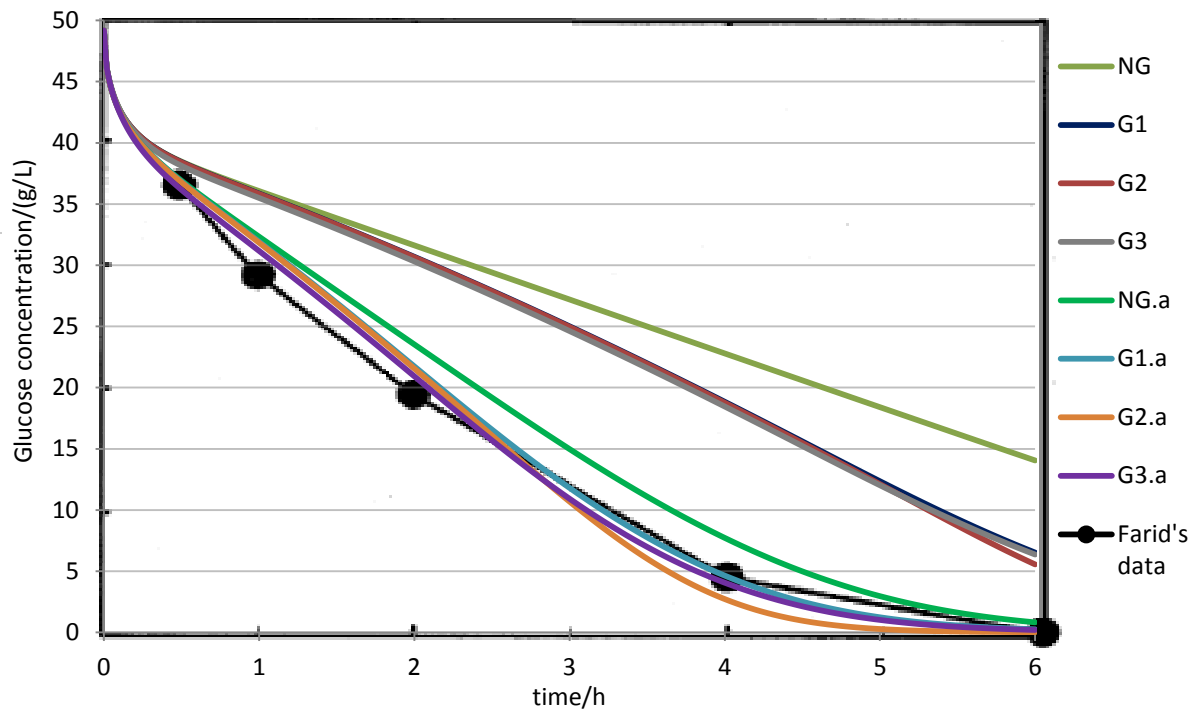


Figure 22. Comparison of glucose batch simulations with experimental values from Talebnia et al [35].

4.3.2 Batch cultivation of glucose and furfural

In order to compare the bulk concentration with the results obtained by Farid Talebnia [35], the concentration of furfural was changed to 5 g/L and the glucose concentration to 40 g/L .

Because of the lack of information regarding the biomass concentration at the end of the fermentation time, it was assumed that the growth would be similar to the one in the previous case. The results for the bulk concentration are presented in *Figure 23* and *Figure 24*.

Visualizing the figures, it can be concluded that both glucose and furfural were consumed faster in all the models than in the experimental setup. This may have happened because of the non-consideration of external mass transfer resistances in this work, a fact that would cause a rapid transport in the starting point of consumption and an absence of a mass transfer resistance in all the fermentation time.

The model that fits the experimental data best is NG.a, which is the model that didn't consider the growth of the cells. This could mean that furfural is highly inhibiting the growth of the cells. Between model G1, G2 and G3, the one that fits the glucose and furfural consumption better is G1, but the difference between the concentrations profiles are very low.

In each model, the change of q_{max} (0.01 mol/(g h) to 0.006 mol/(g h)) resulted in better fit to data values.

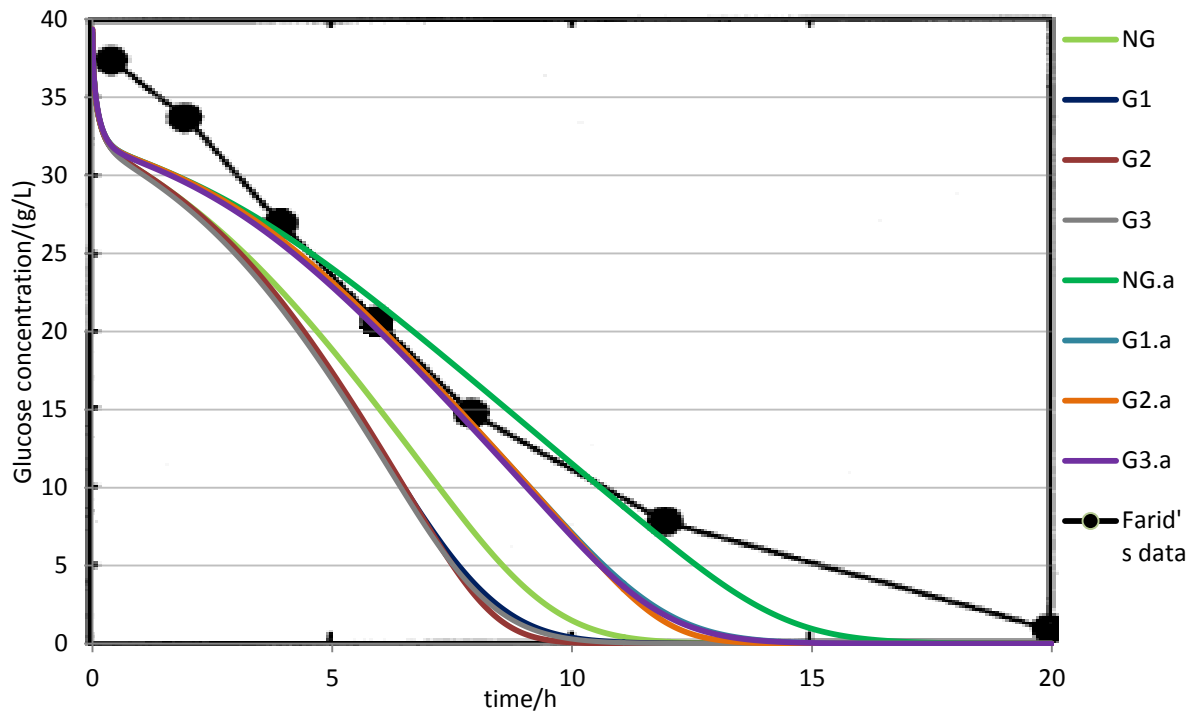


Figure 23. Concentration of glucose in batch fermentation with furfural [5 g/L]. In black are the results obtained by Talebnia et al [35].

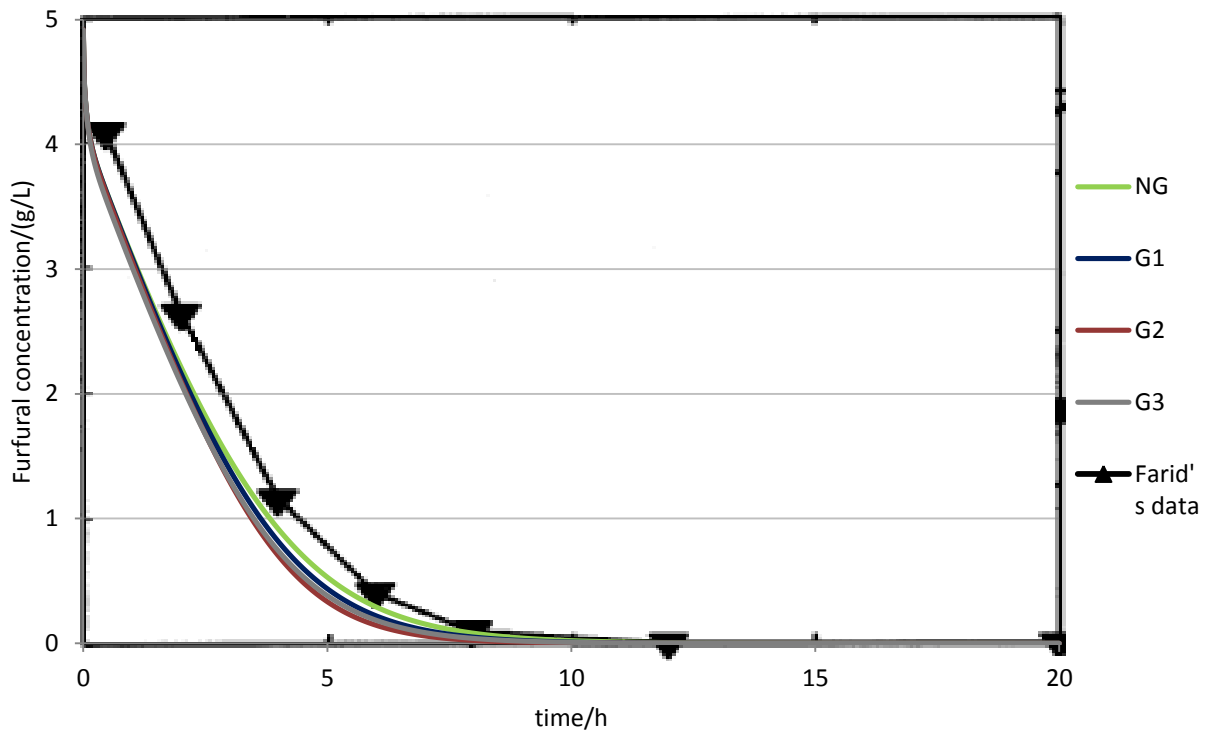


Figure 24. Concentration of Furfural in batch fermentation with glucose [40 g/L]. The line in black are the results obtained by Talebnia et al [35].

4.4 Sensitivity analysis

In this part of the report, effects of the variation of the formulation inputs on the results and the variation of the parameter on the variables were studied. This can be also important when it refers to understand the weight of the parameters in the formulation.

The variation effects were studied with the aid of the COMSOL's tool parametric sweep. This tool offers the possibility to test different values for a parameter.

Control coefficients were also calculated for all the kinetic and diffusion parameters in model 4 for $t = 1500$ s and for $t = 86400$ s. The times were chosen to study the variation of these coefficients before and in the steady state. The control coefficients were calculated based on the Metabolic Control Analysis theory, *APPENDIX G* [36][37]. These coefficients were obtained for glucose and xylose consumption rate.

4.4.1 K_{si} variation effects in the consumption rate and the efficiency factor

Figure 25 shows the relation between the efficiency factor for glucose and xylose and the K_{si} (the variation was done for furfural and HMF at the same time) for model 4.

k is the variable used to define the factor which was multiplied by K_i and then tested, *Table 6*. Note that k equal to 1 corresponds to the inhibition constants used in the Continuous fermentation studies.

In the graphic representation of the efficiency factor for glucose, we can verify that for smaller inhibition constants (high inhibition effects) the encapsulation is beneficial for the glucose consumption. The cells are protected inside the cell pellet, and are also subject of lower concentration of inhibitors. As the inhibitory effects decrease, it becomes less advantageous for the cell to be encapsulated and mass transfer limitations become more important. k equal to 1.7 is the turn-over point.

Xylose plot fits the theory mentioned in the previous paragraph, but for this case, encapsulation is always advantageous for xylose consumption.

Table 6. k and respective values for the inhibition constants. k equal to 1 corresponds to the values of K_{si} used in the initial formulation

k	$\frac{K_{fi}}{\text{mol/m}^3}$	$\frac{K_{hi}}{\text{mol/m}^3}$
0.01	0.028	0.634
0.1	2.08	6.34
1	20.8	63.4
5	104	317
10	208	634

*Note: k , studied variable; K_{fi} , inhibition constant for furfural; K_{hi} , inhibition constant for HMF.

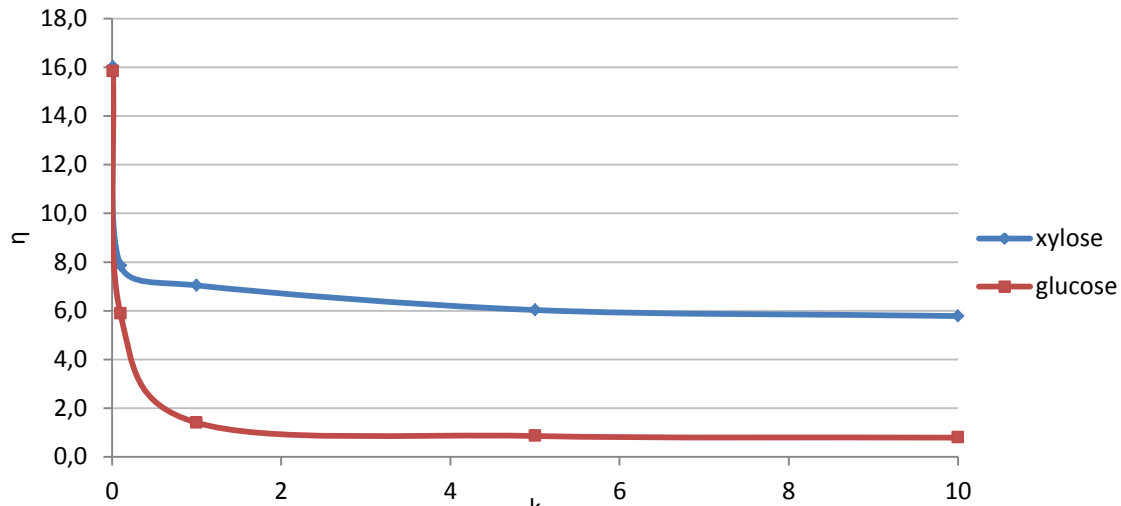


Figure 25. η versus k . Parametric sweep results for testing different values of K_{si} for furfural and HMF.

In this situation, even when the inhibition effect of furfural and HMF is lower, the xylose consumption is benefited by the protection caused by glucose mass transfer limitations.

4.4.2 K_{si} and D_{sc} variation effects in the efficiency factor

Figure 26 and Figure 27 show the results for K_{si} and D_{sc} variation effects in η . Five values of k were tested for five values of D_{sc} , Table 7. Note that $D_{sc} = 0.5D_{sw}$ is the value used in the Continuous fermentation studies, $b = 1$.

As it can be seen, for lower values of k (high inhibition effects) and for smaller values of b (lower diffusion in the cell pellet), the variation of the efficiency factor is higher and it achieves values close to 27, meaning that the encapsulation is extremely beneficial.

In the opposite, for high values of k and high values of b , the benefit of the encapsulation decreases. This means that the inhibitory effect is not so significant in the reaction of consumption, and the diffusion becomes more important.

It can be said that xylose consumption rate is more sensitive to these variations than glucose consumption rate.

Table 7. b and respective values for the diffusion coefficients in the cell pellet. b equal to 1 corresponds to the values of D_{sc} used in the initial formulation

b	$\frac{D_{sc}}{m^2/s}$
0.7	$0.35D_{sw}$
1	$0.5D_{sw}$
1.3	$0.65D_{sw}$
1.7	$0.85D_{sw}$
2	D_{sw}

*Note: b , studied variable; D_{sc} , substrate diffusion coefficient in the cell pellet.

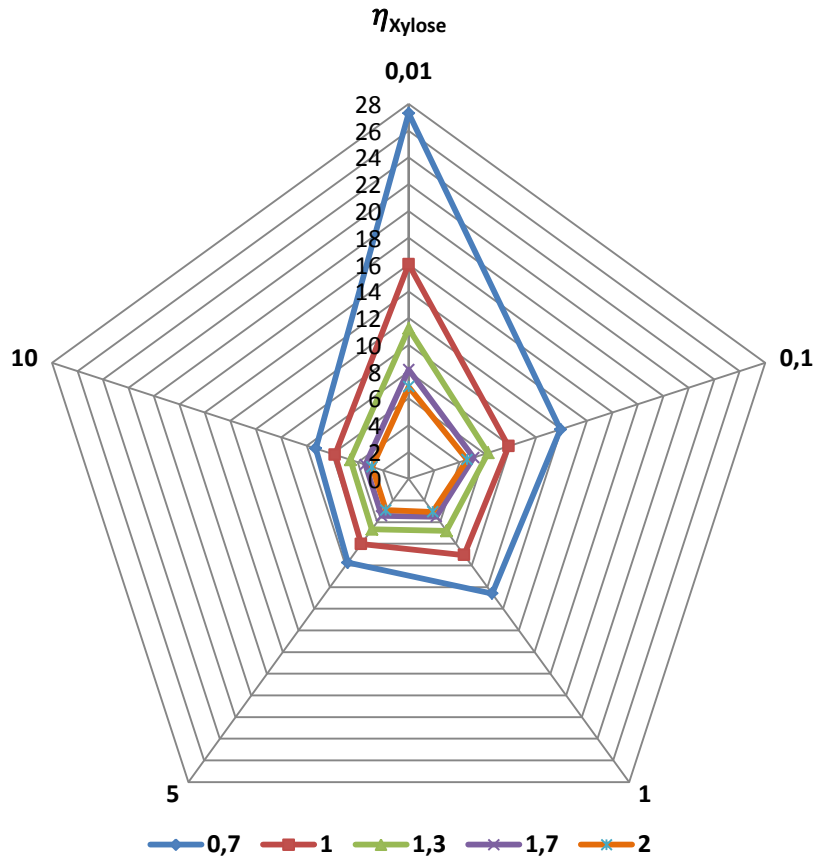


Figure 26. Representation of the variation of η for xylose, when K_{si} and D_{sc} are changed. The distance for the center represents the axis for η , the extreme points of the pentagon are the values of k and the legend of the series stands for the values of b .

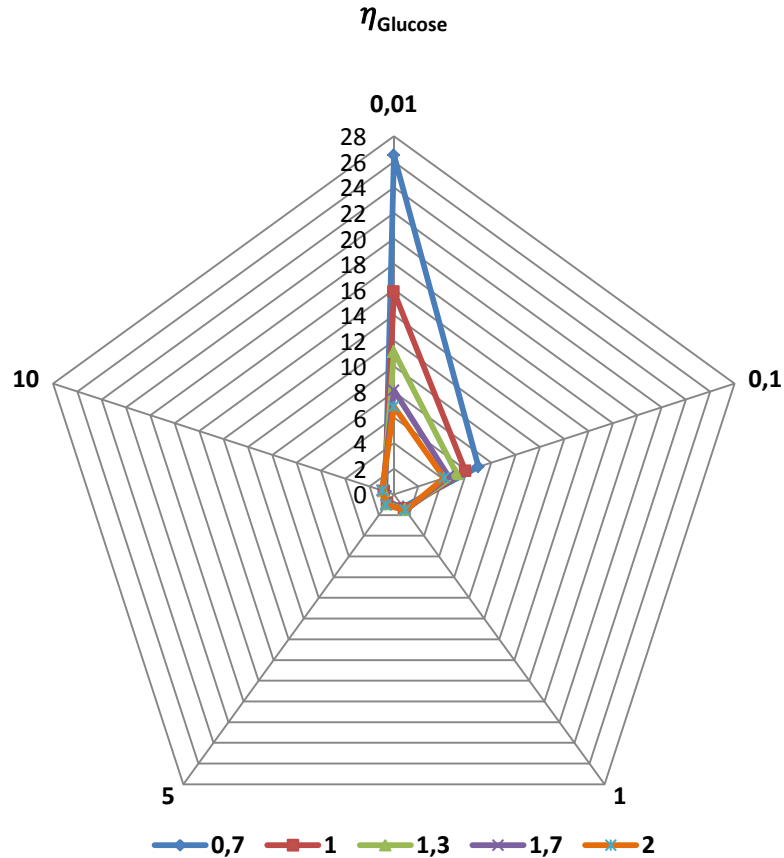


Figure 27. Representation of the variation of η for glucose, when K_{si} and D_{sc} are changed. The distance for the center represents the axis for η , the extreme points of the pentagon are the values of k and the legend of the series stands for the values of b .

4.4.3 q_{xmax} variation effects in the efficiency factor

Table 8 presents the values of m , and the respective values of q_{xmax} . As was previously done, m is the factor multiplied to the original value of q_{xmax} , in order to obtain the new value. So, for $m = 1$, q_{xmax} is the value used in the formulation of model 1 to 4.

Table 9 and Table 10 are the results obtained from the parametric sweep.

Table 8. m and the values for the maximum xylose consumption rate constant. m equal to 1 corresponds to the values of q_{xmax} used in the initial formulation

m	$\frac{q_{xmax}}{mol/(g\ h)}$
0.8	0.0008
0.9	0.0009
1	0.001
1.1	0.0011
1.2	0.0012

*Note: m , studied variable; q_{xmax} , maximum xylose consumption rate constant.

Table 9. Values of glucose reaction rate and efficiency factor for different values of m

m	$\frac{-r_g \times 10^1}{mol/(m^3\ s)}$	$\frac{-r_{gmax.dif} \times 10^1}{mol/(m^3\ s)}$	η
0.8	1.7551	1.4436	1.2158
0.9	1.7552	1.4436	1.2159
1	1.7554	1.4436	1.2160
1.1	1.7555	1.4436	1.2161
1.2	1.7557	1.4436	1.2162

*Note: m , studied variable; $-r_g$, glucose reaction rate at normal conditions; $-r_{gmax.dif}$, glucose reaction rate in the maximum diffusion case; η , efficiency factor.

Table 10. Reaction rate and efficiency factor for xylose consumption for m values

m	$\frac{-r_x \times 10^3}{mol/(m^3\ s)}$	$\frac{-r_{xmax.dif} \times 10^4}{mol/(m^3\ s)}$	η
0.8	1.5500	5.9553	2.6027
0.9	1.7421	6.6997	2.6002
1	1.9338	7.4440	2.5978
1.1	2.1251	8.1884	2.5953
1.2	2.3161	8.9327	2.5929

*Note: m , studied variable; $-r_x$, xylose reaction rate at normal conditions; $-r_{xmax.dif}$, xylose reaction rate in the maximum diffusion case; η , efficiency factor.

It can be seen that an increase of q_{xmax} results in a decrease of the efficiency factor for xylose and an increase for glucose.

It can also be observed that an increase of 10 % of q_{xmax} , for example, from $q_{xmax} = 0.001 \text{ mol}/(\text{m}^3 \text{ s})$ to $q_{xmax} = 0.0011 \text{ mol}/(\text{m}^3 \text{ s})$, causes an increase of the consumption rate of 0.008 % for glucose and 9.9 % of xylose. In this case, the increase of the efficiency factor was approximately 0.008 % for glucose while the efficiency factor for xylose decreased 0.09 %.

Summarizing, xylose consumption rate is almost directly dependent on q_{xmax} , while the efficiency factor is almost completely insensitive to changes in this parameter.

4.4.4 Control coefficient for q_{smax}

Table 11 and Table 12 display the results of control coefficients of q_{gmax} , q_{xmax} , q_{fmax} and q_{hmax} on glucose and xylose consumption reaction. See also APPENDIX G.

For all q_{smax} , when an increment of the values happens, it causes an increase in $-r_g$ and $-r_x$, meaning that the reaction of consumption increases.

Table 11. Control coefficient of q_{smax} over $-r_g$

Parameter changed	$C_{q_{smax}}^{-r_g}, t = 1500 \text{ s}$	$C_{q_{smax}}^{-r_g}, t = 86400 \text{ s}$
q_{gmax}	0.8789	0.8749
q_{xmax}	0.0009	0.0008
q_{fmax}	0.0715	0.0713
q_{hmax}	0.0148	0.0165

*Note: q_{gmax} , maximum glucose consumption rate constant; q_{xmax} , maximum xylose consumption rate constant; q_{fmax} , maximum furfural consumption rate constant; q_{hmax} , maximum HMF consumption rate constant; $-r_g$, glucose reaction rate; $C_{q_{smax}}^{-r_g}$, control coefficient of q_{smax} over $-r_g$.

Table 12. Control coefficient of q_{smax} over $-r_x$

Parameter changed	$C_{q_{smax}}^{-r_x}, t = 1500 \text{ s}$	$C_{q_{smax}}^{-r_x}, t = 86400 \text{ s}$
q_{gmax}	0.8829	0.9806
q_{xmax}	0.9883	0.9905
q_{fmax}	0.2099	0.2247
q_{hmax}	0.0667	0.0842

*Note: q_{gmax} , maximum glucose consumption rate constant; q_{xmax} , maximum xylose consumption rate constant; q_{fmax} , maximum furfural consumption rate constant; q_{hmax} , maximum HMF consumption rate constant; $-r_x$, xylose reaction rate; $C_{q_{smax}}^{-r_x}$, control coefficient of q_{smax} over $-r_x$.

It can be seen that glucose consumption is mostly dependent on the maximum glucose consumption rate constant, while xylose consumption is strongly dependent on the maximum consumption rate constants of glucose and xylose, and it is also affected by the maximum furfural consumption rate constant.

4.4.5 Control coefficient for K_s

The same procedure was followed to obtain the control coefficients for the Monod constant for all the substrates and inhibitors, as it is explained in *APPENDIX G*.

Table 13 and *Table 14* contain the results achieved.

For K_g , K_x , K_f and K_h , it can be concluded that an increase of these values, meaning a decrease of the affinity for the substrate or inhibitor, causes a decrease of $-r_g$.

For $-r_x$, an increase of K_g , K_x , K_f and K_h causes a decrease of this value.

K_s values have a higher control over xylose consumption rate than over glucose. K_g is the parameter that has a greater control over $-r_g$, and for $-r_x$ is K_x .

For all $C_{q_{max}}^{-r_s}$, the control coefficient values are higher at $t = 86400$ s meaning that in the stationary state, a variation of K_s causes a higher variation of the consumption reaction when

Table 13. Control coefficient of K_s over $-r_g$

Parameter changed	$C_{K_s}^{-r_g}, t = 1500$ s	$C_{K_s}^{-r_g}, t = 86400$ s
K_g	-0.0749	-0.0753
K_x	-0.0006	-0.0006
K_f	-0.0469	-0.0468
K_h	-0.0109	-0.0119

*Note: K_g , saturation constant for glucose; K_x , saturation constant for xylose; K_f , saturation constant for furfural, K_h , saturation constant for HMF; $-r_g$, glucose reaction rate; $C_{K_s}^{-r_g}$, control coefficient of K_s over $-r_g$.

Table 14. Control coefficient of K_s over $-r_x$

Parameter changed	$C_{K_s}^{-r_x}, t = 1500$ s	$C_{K_s}^{-r_x}, t = 86400$ s
K_g	-0.1971	-0.2060
K_x	-0.7949	-0.8216
K_f	-0.1489	-0.1591
K_h	-0.0501	-0.0613

*Note: K_g , saturation constant for glucose; K_x , saturation constant for xylose; K_f , saturation constant for furfural, K_h , saturation constant for HMF; $-r_x$, xylose reaction rate; $C_{K_s}^{-r_x}$, control coefficient of K_s over $-r_x$.

compared with the values at $t = 1500$ s.

4.4.1 Control coefficient for K_{si}

The effects of variation of the inhibition constant in the glucose and xylose consumption were analyzed and the results are presented in *Table 15* and *Table 16*.

As it can be seen, for all cases, an increase of K_{si} , in other words, a decrease of the inhibitory effect, causes an increase of glucose and xylose consumption rate.

Xylose consumption rate is more sensitive to the inhibition constants than glucose consumption rate.

Between furfural and HMF inhibition constants, the one that has a greater control over $-r_g$ is K_{fi} .

Table 15. Control coefficient of K_{si} over $-r_g$

Parameter changed	$C_{K_{si}}^{-r_g}, t = 1500$ s	$C_{K_{si}}^{-r_g}, t = 86400$ s
K_{gi}	0.0005	0.0006
K_{xi}	0.0650	0.0659
K_{fi}	0.3138	0.3119
K_{hi}	0.1583	0.1592

*Note: K_{gi} , inhibition constant for glucose; K_{xi} , inhibition constant for xylose; K_{fi} , inhibition constant for furfural; K_{hi} , inhibition constant for HMF; $-r_g$, glucose reaction rate; $C_{K_{si}}^{-r_g}$, control coefficient of K_{si} over $-r_g$.

Table 16. Control coefficient of K_{si} over $-r_x$

Parameter changed	$C_{K_{si}}^{-r_x}, t = 1500$ s	$C_{K_{si}}^{-r_x}, t = 86400$ s
K_{gi}	0.7578	0.7967
K_{xi}	0.1629	0.1788
K_{fi}	0.3123	0.3311
K_{hi}	0.2802	0.3103

*Note: K_{gi} , inhibition constant for glucose; K_{xi} , inhibition constant for xylose; K_{fi} , inhibition constant for furfural; K_{hi} , inhibition constant for HMF; $-r_x$, xylose reaction rate; $C_{K_{si}}^{-r_x}$, control coefficient of K_{si} over $-r_x$.

4.4.2 Control coefficient for D_{sc}

Table 17 and Table 18 contain the values of $C_{D_{sc}}^{-r_s}$. These values are the control coefficients of the diffusion coefficients in the cell pellet on the glucose and xylose consumption rate.

From the observation of Table 17 it can be emphasized that when the value of D_{sc} increases, $-r_g$ increases for D_{gc} and decreases for the others.

When the diffusion coefficients of xylose, furfural and HMF increase, there is a greater presence of these inside the capsule, contributing to the reduction of the reaction rate.

Between the values for $t = 1500 s$ and for $t = 86400 s$ it can be seen that all the effects are in the same direction and the quantitative difference is generally rather small.

$-r_x$ increases when D_{xc} has increases too. The increase of the remaining ones causes a decrease of the xylose consumption. The higher amount of glucose, furfural and HMF will lead to a higher inhibitory effect over xylose consumption.

Table 17. Control coefficient of D_{sc} over $-r_g$

Parameter changed	$C_{D_{sc}}^{-r_g}, t = 1500 s$	$C_{D_{sc}}^{-r_g}, t = 86400 s$
D_{gc}	0.0920	0.0842
D_{xc}	-0.0058	-0.0005
D_{fc}	-0.0123	-0.0121
D_{hc}	-0.0086	-0.0070

*Note: D_{gc} , diffusion coefficient of glucose in the cell pellet; D_{xc} , diffusion coefficient of xylose in the cell pellet; D_{fc} , diffusion coefficient of furfural in the cell pellet; D_{hc} , diffusion coefficient of HMF in the cell pellet ; $-r_g$, glucose reaction rate; $C_{D_{sc}}^{-r_g}$, control coefficient of D_{sc} over $-r_g$.

Table 18. Control coefficient of D_{sc} over $-r_x$

Parameter changed	$C_{D_{sc}}^{-r_x}, t = 1500 s$	$C_{D_{sc}}^{-r_x}, t = 86400 s$
D_{gc}	-0.6635	-0.6638
D_{xc}	0.0784	0.0063
D_{fc}	-0.1041	-0.1093
D_{hc}	-0.0638	-0.0540

*Note: D_{gc} , diffusion coefficient of glucose in the cell pellet; D_{xc} , diffusion coefficient of xylose in the cell pellet; D_{fc} , diffusion coefficient of furfural in the cell pellet; D_{hc} , diffusion coefficient of HMF in the cell pellet ; $-r_x$, xylose reaction rate; $C_{D_{sc}}^{-r_x}$, control coefficient of D_{sc} over $-r_x$.

The results from the sensitivity analysis allow concluding that xylose conversion is rate-limited (i.e. any parameter change that increases the xylose reaction rate will increase the overall xylose consumption), while glucose consumption is diffusion-limited (meaning that an increase in the reaction rate will not cause a significant increase in the glucose consumption, since the diffusion will limit the transport into the capsule, the effect will instead be a lower concentration within the pellet).

5. CONCLUSIONS

After the elaboration of this report, it can be said that COMSOL Multiphysics is a good tool to simulate and study bioprocesses.

Glucose and xylose co-consumption and inhibition effects of furfural and HMF were studied. Glucose, in presence of xylose and inhibitors, suffers a reduction of 25.1 % of the consumption rate. Only 12.2 % of xylose is consumed in presence of 40 g/L of glucose. When inhibitors were added, this percentage of consumption decreased to 6.5 %.

Evaluating the efficiency factor, it can be concluded that xylose is the component that most benefits with the encapsulation.

The turn-over point for glucose, meaning the point where it is no longer favorable for the glucose consumption to happen in immobilized cells, occurs to a K_{fi} equal to 35.4 mol/m^3 and to a K_{hi} equal to 107.8 mol/m^3 . This results in a combined inhibitory effect of 45.1 % in glucose consumption. For higher values of inhibition constants, the diffusion limitations have a higher weight than the kinetic inhibition.

Validation of the models was performed using Farid Talebnia's published data. In the case of glucose fermentation in synthetic medium, the model that fitted better was G1.a and G3.a (with the changed q_{max}). For the batch fermentations of glucose in presence of 5 g/L of furfural, the model that had a lower difference with the data was the model that didn't consider the growth, meaning a high inhibition of cells growth caused by furfural.

With the sensitivity analysis tool it was possible to know that for all K_{si} values, cell encapsulation is always beneficial for xylose. Comparatively, the glucose is only benefited by the encapsulation in presence of high inhibition effects.

For K_{si} and D_{sc} variation effects, xylose consumption rate is extremely sensitive when compared with the glucose consumption rate. For glucose, the diffusion problems became more important than inhibition when the inhibition constants have high values.

When the variation effects of q_{xmax} were studied, it could be seen that xylose consumption rate is linearly dependent on this parameter, however the efficiency factor is almost insensitive to changes in this variable.

Generally, the sensitivity of the consumption rate of xylose to q_{smax} , K_s , K_{si} , D_{sc} is higher than that of glucose consumption.

For q_{smax} , the reaction rate of glucose is mostly controlled by q_{gmax} and the reaction rate of xylose is mostly dependent on q_{gmax} and q_{xmax} .

For K_s , the reaction rates of glucose and xylose are more sensitive to K_g and K_x , respectively.

The sensitivity study on the inhibition constants show that, glucose consumption rate is more sensitive to K_{xi} and xylose consumption rate is more influenced by K_{gi} variations.

Finally, both glucose and xylose reaction rate are more sensitive to D_{gc} .

6. FUTURE WORK

Although including the effect of inhibitors and xylose and glucose co-consumption, the formulation applied is quite simple, but still can be improved. We think that it will be a source of improvement to:

- i. change the kinetic model to a set of reactions expressing a metabolic network model;
- ii. include the diffusion of the products from the interior of the capsule to the bulk;
- iii. try to validate the concentration profiles inside the capsule through Molecular Microscopy.

The changes on the formulation of the models will add parameters and variables to them. This will have as a result the increase of the computation time needed to solve the problem. Therefore, this should be done in a computer with capacity to deal with a fine mesh and small values of time steps and tolerances.

CONTRIBUTION REPORT

In the *table 7*, are presented the main tasks of the master thesis and the contribution of each student in the project.

Table 19. Tasks and the respective participation of the master's students, (-) stands for less participative and (+) for more

Task	Master's name	
	Gonçalo	Joana
Writing of the Draft planning report	+	+
Formulation of relations and variables to describe the behavior of encapsulated yeast	-	+
Formulation with COMSOL Multiphysics 4.1	+	-
Proceed to validation of the model with publish data and suggestions for validation in new experiments	+	+
Execute parameter sensitivity analysis and tests	+	+
Writing of the report	+	+

REFERENCES

- [1] **M. Yeomans**, *Oil: Anatomy of an Industry*. New Press, The, 2004.
- [2] **E. Gnansounou**, "Production and use of lignocellulosic bioethanol in Europe: Current situation and perspectives," *Bioresource Technology*, vol. 101, no. 13, pp. 4842-4850, Jul. 2010.
- [3] **S. I. Mussatto et al.**, "Technological trends, global market, and challenges of bioethanol production," *Biotechnology Advances*, vol. 28, no. 6, pp. 817-830, Nov. 2010.
- [4] **A. Eisentraut**, "SUSTAINABLE PRODUCTION OF SECOND-GENERATION BIOFUELS." IEA International Energy Agency, Jul. 2010.
- [5] **G. M. Walker**, *Bioethanol: Science and technology of fuel alcohol*. Ventus Publishing ApS, 2010.
- [6] **R. A. Lestari**, "Modeling of Concentration Profiles in Yeast Capsules for Efficient Bioethanol Production," Master of Science Thesis, Chalmers University of Technology, Göteborg, Sweden, 2010.
- [7] **B. Giri et al.**, "Commercializing lignocellulosic bioethanol: technology bottlenecks and possible remedies," *Biofuels, bioproducts & biorefining*, vol. 4, no. 1, pp. 77-93, Jan. 2010.
- [8] **B. Hahn-Hägerdal and L. Olsson**, "Fermentation of lignocellulosic hydrolysates for ethanol production," *Enzyme and microbial technology*, vol. 18, no. 5, pp. 312-331, Apr. 1996.
- [9] **A. Nag**, *Biofuels Refining and Performance*. New York: McGraw-Hill, 2008.
- [10] **E. Palmqvist**, "Fermentation of lignocellulosic hydrolysates. II: inhibitors and mechanisms of inhibition," *Bioresource technology*, vol. 74, no. 1, pp. 25-33, Aug. 2000.
- [11] **M. Moo Young, W. A. Anderson, and F. W. Bai**, "Ethanol fermentation technologies from sugar and starch feedstocks," *Biotechnology advances*, vol. 26, no. 1, pp. 89-105, Jan. 2008.
- [12] **K. Karhumaa, R. G. Sanchez, B. Hahn-Hägerdal, and M.-F. Gorwa-Grauslund**, "Comparison of the xylose reductase-xylitol dehydrogenase and the xylose isomerase pathways for xylose fermentation by recombinant *Saccharomyces cerevisiae*," *Microbial Cell Factories*, vol. 6, pp. 5-5, Feb. 2007.
- [13] **T. Modig, M. Gorwagrauslund, G. Lidén, J. Almeida, B. Hahn-Hägerdal, and A. Petersson**, "Increased tolerance and conversion of inhibitors in lignocellulosic hydrolysates by *Saccharomyces cerevisiae*," *Journal of chemical technology and biotechnology*, Jan. 2007.
- [14] **K. H. Huebner**, *The Finite Element Method for Engineers*, 4th ed. New York: Wiley, 2001.
- [15] **G. R. Liu**, *Finite Element Method a Practical Course*. Oxford: Butterworth-Heinemann, 2003.
- [16] **N. Ottosen and H. Petersson**, *Introduction to the Finite Element Method*. New York: Prentice Hall, 1992.
- [17] **E. L. Cussler**, *Diffusion: Mass Transfer in Fluid Systems*, 2nd ed. Cambridge: Cambridge Univ. Press, 1997.

- [18] **D. Basmadjian**, “More About Mass, Energy, and Momentum Balances,” in *The Art of Modeling in Science and Engineering*, CRC Press, 1999, pp. 13-18.
- [19] **G. Birol, P. Doruker, B. Kirdar, Z. Ilsen, and K. Ülgen**, “Mathematical description of ethanol fermentation by immobilised *Saccharomyces cerevisiae*,” *Process Biochemistry*, vol. 33, no. 7, pp. 763-771, Sep. 1998.
- [20] **M. Bertilsson, J. Andersson, and G. Lidén**, “Modeling simultaneous glucose and xylose uptake in *Saccharomyces cerevisiae* from kinetics and gene expression of sugar transporters,” *Bioprocess and Biosystems Engineering*, vol. 31, no. 4, pp. 369-377, Nov. 2007.
- [21] **J. Shi, Ed.**, “Microbial Modeling as Basis for Bioreactor Design for Nutraceutical Production,” in *Functional Food Ingredients and Nutraceuticals*, Taylor & Francis Group, LLC, 2007, pp. 239-251.
- [22] **T. Lebeau, T. Jouenne, and G.-A. Junter**, “Diffusion of Sugars and Alcohols Through Composite Membrane Structures Immobilizing Viable Yeast Cells,” *Enzyme and Microbial Technology*, vol. 22, no. 6, pp. 434-438, May 1998.
- [23] **A. A. Vicente, M. Dluhý, E. C. Ferreira, M. Mota, and J. A. Teixeira**, “Mass transfer properties of glucose and O₂ in *Saccharomyces cerevisiae* flocs,” *Biochemical Engineering Journal*, vol. 2, no. 1, pp. 35-43, Sep. 1998.
- [24] **Y.-H. Weng et al.**, “Separation of furans and carboxylic acids from sugars in dilute acid rice straw hydrolyzates by nanofiltration,” *Bioresource Technology*, vol. 101, no. 13, pp. 4889-4894, Jul. 2010.
- [25] **F. Talebnia and M. J. Taherzadeh**, “In situ detoxification and continuous cultivation of dilute-acid hydrolyzate to ethanol by encapsulated *S. cerevisiae*,” *Journal of Biotechnology*, vol. 125, no. 3, pp. 377-384, Sep. 2006.
- [26] **F. Talebnia and M. J. Taherzadeh**, “Physiological and morphological study of encapsulated *Saccharomyces cerevisiae*,” *Enzyme and Microbial Technology*, vol. 41, no. 6-7, pp. 683-688, Nov. 2007.
- [27] **B. Teusink et al.**, “Can yeast glycolysis be understood in terms of in vitro kinetics of the constituent enzymes? Testing biochemistry,” *European Journal of Biochemistry / FEBS*, vol. 267, no. 17, pp. 5313-5329, Sep. 2000.
- [28] **F. Hynne, S. Danø, and P. G. Sørensen**, “Full-scale model of glycolysis in *Saccharomyces cerevisiae*,” *Biophysical Chemistry*, vol. 94, no. 1-2, pp. 121-163, Dec. 2001.
- [29] **M. Kuyper, M. J. Toirkens, J. A. Diderich, A. A. Winkler, J. P. van Dijken, and J. T. Pronk**, “Evolutionary engineering of mixed-sugar utilization by a xylose-fermenting *Saccharomyces cerevisiae* strain,” *FEMS Yeast Research*, vol. 5, no. 10, pp. 925-934, Jul. 2005.
- [30] **I. S. Horváth, M. J. Taherzadeh, C. Niklasson, and G. Lidén**, “Effects of furfural on anaerobic continuous cultivation of *Saccharomyces cerevisiae*,” *Biotechnology and Bioengineering*, vol. 75, no. 5, pp. 540-549, Dec. 2001.
- [31] **M. J. Taherzadeh, L. Gustafsson, C. Niklasson, and G. Lidén**, “Physiological effects of 5-hydroxymethylfurfural on *Saccharomyces cerevisiae*,” *Applied Microbiology and Biotechnology*, vol. 53, no. 6, pp. 701-708, Jun. 2000.

- [32] **M. Kuyper et al.**, “High-level functional expression of a fungal xylose isomerase: the key to efficient ethanolic fermentation of xylose by *Saccharomyces cerevisiae*?,” *FEMS Yeast Research*, vol. 4, no. 1, pp. 69-78, Oct. 2003.
- [33] **M. S. Krishnan, N. W. Y. Ho, and G. T. Tsao**, “Fermentation Kinetics of Ethanol Production from Glucose and Xylose by Recombinant *Saccharomyces* 1400(pLNH33),” *Applied Biochemistry and Biotechnology*, vol. 78, no. 1-3, pp. 373-388, 1999.
- [33] **COMSOL AB**, “COMSOL Multiphysics Modeling Guide VERSION 3.5a.” COMSOL AB, Nov. 2008.
- [35] **F. Talebnia, C. Niklasson, and M. J. Taherzadeh**, “Ethanol production from glucose and dilute-acid hydrolyzates by encapsulated *S. cerevisiae*,” *Biotechnology and Bioengineering*, vol. 90, no. 3, pp. 345-353, May 2005.
- [36] **R. Moreno-Sánchez, E. Saavedra, S. Rodríguez-Enríquez, and V. Olín-Sandoval**, “Metabolic Control Analysis: A Tool for Designing Strategies to Manipulate Metabolic Pathways,” *Journal of Biomedicine and Biotechnology*, vol. 2008, 2008.
- [37] **P. Mendes**, “MCA - Control Coefficients,” *The University of Manchester*, 1995. [Online]. Available: http://dbkgroup.org/metab/mca_cc.htm. [Accessed: 10-Jul-2011].
- [38] “Wolfram|Alpha: Computational Knowledge Engine.” [Online]. Available: <http://www.wolframalpha.com/>. [Accessed: 12-Jun-2011].
- [39] **G. Stephanopoulos, A. A. Aristidou, J. H. Nielsen, and J. Nielsen**, *Metabolic engineering: principles and methodologies*. Academic Press, 1998.
- [40] **F. Talebnia**, “Ethanol Production from Cellulosic Biomass by Encapsulated *Saccharomyces cerevisiae*. Ph.D dissertation.” Chalmers University of Technology, Dep. of Chemical and Biological Engineering, 2008.
- [41] **S. H. Cheong, J. K. Park, B. S. Kim, and H. N. Chang**, “Microencapsulation of yeast cells in the calcium alginate membrane,” *Biotechnology Techniques*, vol. 7, no. 12, pp. 879-884, Dec. 1993.
- [42] **E. W. Weisstein**, “Spherical Segment -- from Wolfram MathWorld.” [Online]. Available: <http://mathworld.wolfram.com/SphericalSegment.html>. [Accessed: 11-Jun-2011].
- [43] **E. W. Weisstein**, “Spherical Cap -- from Wolfram MathWorld.” [Online]. Available: <http://mathworld.wolfram.com/SphericalCap.html>. [Accessed: 01-Jun-2011].

APPENDIX

APPENDIX A - Formulations

In this appendix, the formulations for model 1 to 3 are presented.

A.1 - Model 1: Glucose consumption

- Consumption

In order to ignore the effect of the growth, a variable v_{max} was created – just uptake capacity.

$$R_g = v_{gmax} \frac{C_g}{C_g + K_g} \quad (64)$$

Where:

$$v_{gmax} = q_{gmax}X \quad (65)$$

- Diffusion

$$N_g = -D_g \frac{dC_g}{dr} \quad (66)$$

- Global Balance [18]

$$\left(\text{Rate of Glucose in} \right) - \left(\text{Rate of Glucose out} \right) - \left(\text{Rate of consumption} \right) = \left(\text{Rate of accumulation} \right) \quad (67)$$

$$N'_g|_{r+\Delta r} - N'_g|_r - R_g \Delta V = \Delta V \frac{dC_g}{dt} \quad (68)$$

And,

$$N'_g = -N_g A \quad (69)$$

$$N'_g = - \left(-D_g A \frac{dC_g}{dr} \right) = D_g A \frac{dC_g}{dr} \quad (70)$$

In the limit,

$$dN'_g - R_g dV = dV \frac{dC_g}{dt} \quad (71)$$

$$d \left(D_g 4\pi r^2 \frac{dC_g}{dr} \right) - R_g 4\pi r^2 dr = 4\pi r^2 dr \frac{dC_g}{dt} \quad (72)$$

Differential of a product,

$$D_g \left(8\pi r \frac{dC_g}{dr} + 4\pi r^2 \frac{d^2 C_g}{dr^2} \right) - R_g 4\pi r^2 dr = 4\pi r^2 dr \frac{dC_g}{dt} \quad (73)$$

Dividing for D and $4\pi r^2 dr$,

$$\frac{2}{r} \frac{dC_g}{dr} + \frac{d^2 C_g}{dr^2} - \frac{R_g}{D_g} = \frac{1}{D_g} \frac{dC_g}{dt} \quad (74)$$

$$r = 0 \rightarrow \frac{dC_g}{dr} = 0$$

$$r = R \rightarrow C_g = C_{gbulk}$$

A.2 - Model 2: Glucose and Xylose co-consumption

- Consumption [20]

Glucose

$$R_g = v_{gmax} \frac{C_g}{K_g \left(1 + \frac{C_x}{K_{xi}} \right) + C_g} \quad (75)$$

Xylose

$$R_x = v_{xmax} \frac{C_x}{K_x \left(1 + \frac{C_g}{K_{gi}} \right) + C_x} \quad (76)$$

Where:

$$v_{xmax} = q_{xmax} X \quad (77)$$

- Diffusion

Substituting N'_g for N'_j :

$$N'_j = D_j A \frac{dC_j}{dr} \quad (78)$$

- Global balance

$$D_j \left(\frac{2}{r} \frac{dC_j}{dr} + \frac{d^2 C_j}{dr^2} \right) - R_j = \frac{dC_j}{dt} \quad (79)$$

$$r = 0 \rightarrow \frac{dC_j}{dr} = 0$$

$$r = R \rightarrow C_j = C_{jbulk}$$

$$j = \{g, x\}$$

A.3 - Model 3: Glucose and inhibitors (furfural and HMF)[21]

- Consumption

Glucose

$$R_g = \left(v_{gmax} \frac{C_g}{C_g + K_g} \right) \left(\frac{1}{1 + \frac{C_f}{K_{fi}}} \right) \left(\frac{1}{1 + \frac{C_h}{K_{hi}}} \right) \quad (80)$$

Furfural

$$R_f = \left(v_{fmax} \frac{C_f}{C_f + K_f} \right) \quad (81)$$

HMF

$$R_h = \left(v_{hmax} \frac{C_h}{C_h + K_h} \right) \quad (82)$$

With:

$$v_{fmax} = q_{fmax}X \quad (83)$$

$$v_{hmax} = q_{hmax}X$$

- Diffusion

$$N'_j = D_j A \frac{dC_j}{dr} \quad (84)$$

- Global balance

$$D_j \left(\frac{2}{r} \frac{dC_j}{dr} + \frac{d^2 C_j}{dr^2} \right) - R_j = \frac{dC_j}{dt} \quad (85)$$

$j = \{g, f, h\}$

A.4 - Model 4: Glucose and Xylose co-consumption and inhibitors

- Consumption

Glucose

$$R_g = \left(v_{gmax} \frac{C_g}{K_g \left(1 + \frac{C_x}{K_{xi}} \right) + C_g} \right) \left(\frac{1}{1 + \frac{C_f}{K_{fi}}} \right) \left(\frac{1}{1 + \frac{C_h}{K_{hi}}} \right) \quad (86)$$

Xylose

$$R_x = \left(v_{xmax} \frac{C_x}{K_x \left(1 + \frac{C_g}{K_{gi}} \right) + C_x} \right) \left(\frac{1}{1 + \frac{C_f}{K_{fi}}} \right) \left(\frac{1}{1 + \frac{C_h}{K_{hi}}} \right) \quad (87)$$

Furfural

$$R_f = \left(v_{fmax} \frac{C_f}{C_f + K_f} \right) \quad (88)$$

HMF

$$R_h = \left(v_{hmax} \frac{C_h}{C_h + K_h} \right) \quad (89)$$

- Diffusion

$$N_j' = D_j A \frac{dC_j}{dr} \quad (90)$$

- Global balance and boundary conditions

$$D_j \left(\frac{2}{r} \frac{dC_j}{dr} + \frac{d^2 C_j}{dr^2} \right) - R_j = \frac{dC_j}{dt} \quad (91)$$

$$j = \{g, x, f, h\}$$

A.5 - Model 5: Glucose activation effect

- Consumption

Glucose [20]

$$R_g = v_{gmax} \frac{C_g}{K_g \left(1 + \frac{C_x}{K_{xi}} \right) + C_g} \quad (92)$$

Xylose

It was assumed by the authors of this report that xylose consumption can be described by a function defined by intervals.

$$R_x = \begin{cases} v_{xmax1} \frac{C_x}{K_x + C_x} \left(1 + \alpha \frac{C_g}{K_{gi}} \right), & \text{if } 0 \leq C_g < C_{ga} \\ v_{xmax2} \frac{C_x}{K_x \left(1 + \frac{C_g - C_{ga}}{K_{gi}} \right) + C_x}, & \text{if } C_g \geq C_{ga} \end{cases} \quad (93)$$

Where:

$$\begin{aligned}
v_{xmax1} &= q_{xmax}X \\
v_{xmax2} &= 2 \times q_{xmax}X
\end{aligned}
\tag{94}$$

C_{ga} being the glucose concentration value in which the xylose consumption rate achieves its maximum and α being the value for which the two branches of the equation are equal at C_{ga} .

- Diffusion

$$N'_j = D_j A \frac{dC_j}{dr} \tag{95}$$

- Global balance

$$\begin{aligned}
D_j \left(\frac{2}{r} \frac{dC_j}{dr} + \frac{d^2 C_j}{dr^2} \right) - R_j &= \frac{dC_j}{dt} \\
j &= \{g, x\}
\end{aligned}
\tag{96}$$

APPENDIX B - Mass balance calculation

In *Table B.1* are presented the values of Molar masses used for mass balance calculations [38].

In the report, the Biomass composition and the molar mass assumed were $CH_{1,78}O_{0,60}N_{0,19}$ and 26.07 g/mol [39], respectively.

Table B.1. Molar masses utilized in the calculation of mass balances

Substance	$\frac{M}{g/mol}$
Glucose	180.156
Xylose	150.13
Furfural	96.0841
HMF	126.11

APPENDIX C - Determination of the average volume around each sphere

First, it was assumed that each capsule had accessibility to an average volume corresponding to a spherical geometry - complex.

In batch fermentation, the average volume that surrounds each capsule was determined according to conditions for continuous cultivation of hydrolyzate by encapsulated *S. cerevisiae*, from Farid Talebnia work [40]. So it will be considered that the fermentation was performed by 4.02 g of biomass present in $2.5 \times 10^{-4} m^3$ of capsules, being the total volume of medium $1 \times 10^{-3} m^3$.

Knowing that the volume of a sphere is:

$$V_{sphere} = \frac{4}{3}\pi r^2 \quad (97)$$

The volume of one capsule, $v_{capsule}$, is approximately $3.35E - 08 m^3$.

The number of capsules will be given by the following equation:

$$n_{capsules} = \frac{v_{capsule}}{v_{totalcapsules}} \quad (98)$$

The value obtained is 7460 capsules.

We are interested to know the average volume available that each capsule has during the fermentation. The value of $1.34 \times 10^{-7} m^3/capsule$ was obtained applying the next equation.

$$V_{medium/capsule} = \frac{v_{totalmedium}}{n_{capsules}} \quad (99)$$

Now we consider:

$$V_{complex} = V_{capsule} + V_{medium/capsule} \quad (100)$$

Remembering that the complex is a sphere, the radius of this complex can be calculated. The value achieved was 3.42 mm.

APPENDIX D - Determination of the relation between diffusion and the cell growth inside the cell pellet for G2

The formulation of the relation between the diffusion and the increase of concentration of the biomass inside the sphere, was based on the studies of T. Lebeau et al [22]. They found out that the next equation “satisfactorily describe the influence of the yeast cell concentration of glucose in 4% (w/v) alginate gel plates” [22].

$$D_{ex} = D_e \times \frac{(1 - 0.003X)}{(1 + 0.0015X)} \quad (101)$$

After studying the relation between the ratio of effective diffusivity in the cell-containing gel and the effective diffusivity in the cell-free gel and the cell concentration, *Figure D.1*, it was assumed that the *Eq. (101)* could be used to describe the relation between the diffusion coefficient of glucose and the cell concentration in the cell pellet of the capsule.

This assumption was based on the value of maximum concentration, approximately 333 g/L, obtained with the *Figure D.1*. This value is near to the one obtained by S. Cheong et al [41], 309 g/L, and which we believe to be close to the maximum packing. The cell concentration of 133 g/L corresponded to D_{ex}/D_e equal to 0.5. In this work, for all models, was used this concentration value and ratio between the diffusion coefficients.

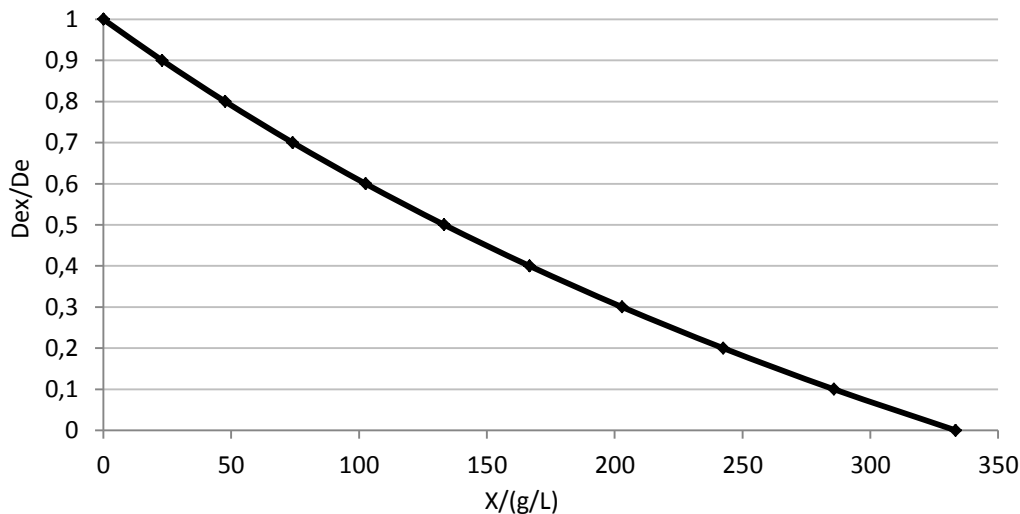


Figure D.1. Graphic representation of the relation expressed by *Eq. (101)* between ratio of effective diffusivity of glucose in the cell-containing gel and the effective diffusivity of glucose in the cell-free gel and the cell concentration in 4% (w/v) alginate gel plates.

APPENDIX E - Determination of the growth equation

To finish the modeling for G2, the equation for biomass growth was still needed. The equation was deduced by a simple analysis of two scenarios - the initial and final states of the fermentation - and the posterior application of Eq. (102).

$$X = X_0 + r_x t \quad (102)$$

E.1 Initial and final characteristics for the glucose fermentation validation [35]

Figure E.1 that pretend to be equivalent in terms of biomass concentration inside the capsule.

In the top, we have the two situations which represent the initial biomass concentration before the growth in G1 (a) and G2 (b). In the bottom it can be seen the two final states of the biomass concentration for G1 (c) and G2 (d).

Note that c and d represent the same concentration of biomass considering the concentration based on the capsule volume. The concentration per cell pellet was obtained by a concentration factor related to the volume differences. From (a) to (c) and (b) to (d), and assuming that the variation of biomass is linear, we get:

From the application of Eq. (102) we get r_x equal to 3.94 g/(L h) for G1 and 1.97 g/(L h) for G2. This simulation was done for 6 h .

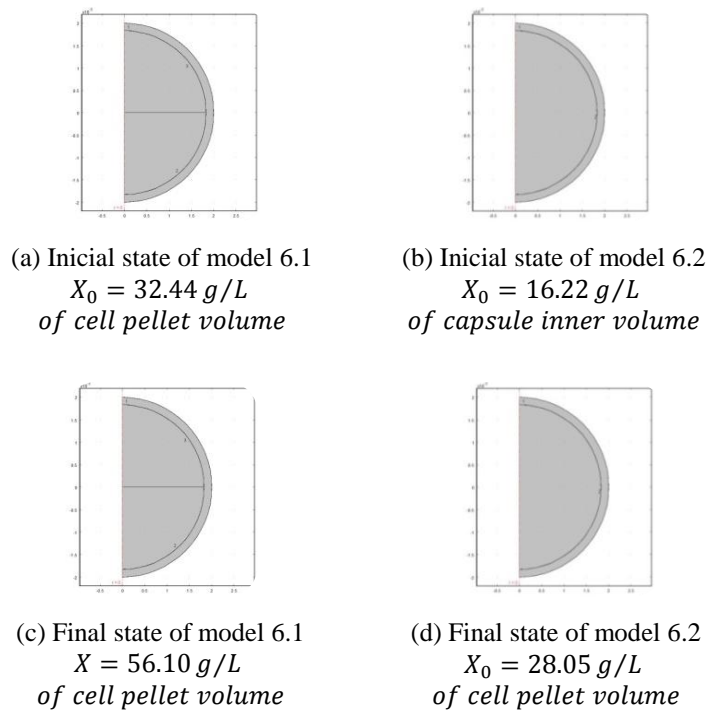


Figure E.1. COMSOL schemes for G1 and G2 for the glucose fermentation validation.

E.2 Initial and final characteristics for the glucose and furfural fermentation validation [35]

For furfural validation, it was assumed that the growth would correspond to the growth of one batch [35]. Therefore the initial and final states are equal to the ones presented in *Figure E.1*. The simulation took 20 *h*.

From *Eq. (102)* we obtained r_x equal to 1.18 *g/(L h)* for G1 and r_x equal to 0.59 *g/(L h)* for G2.

APPENDIX F - Determination of movement velocity of the cell pellet boundary

The idea for the cell growth with the moving boundary was that the boundary would move parallel to the initial position. Each volume variation would have the form of a spherical segment) and the initial volume would have the form of spherical cap. Keeping the volume variation constant, the calculations for the movement velocity of the boundary are then demonstrated.

The 3D geometry, *Figure I.1*, for this situation is presented next.

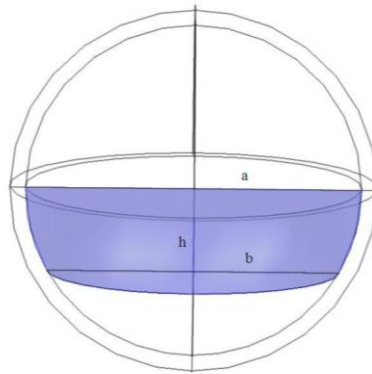


Figure F.1. COMDOL 3D geometry for the idea for cell growth.

The volume of the spherical segment is given by [42].

$$V = \frac{\pi \times h(3a^2 + 3b^2 + h^2)}{6} \quad (103)$$

And the relation between r and b is:

$$radius^2 = h^2 + b^2 \quad (104)$$

To obtain the boundary velocity, the initial volume of the cell pellet has to be calculated. First it was assumed that the final volume would be 20 % of the volume of the cell pellet in G2, meaning 20 % of the inner volume of the capsule.

Knowing the final biomass concentration in G2, the one correspondent to G3 was calculated by *Eq. (105)*. The value obtained was 140.25 g/L.

$$\frac{C_{g_{G2}}}{C_{g_{G3}}} = \frac{V_{G3}}{V_{G2}} \quad (105)$$

Using the same equation for the initial time and knowing that the concentration of biomass is constant in G3, we get $2.96886095715964 \times 10^{-9} m^3$ for the initial volume of cell pellet in G3.

For this initial volume, cap volume [43], the initial height of the boundary should be $1.05093505502527 \times 10^{-2}$ m.

The total volume to fill is $5.13418926315215 \times 10^{-9} m^3$.

F.1 Glucose fermentation

For the glucose fermentation case, the previous volume will be filled in 6 *h*.

The volume variation over time will be $3.60888050998751 \times 10^{-10} m^3/h$. This value was used in Solver (Excel tool) in order to obtain the *h* value for six hours of movement. The curve of velocity as a function of time was obtained and a tendency line was added.

Because of geometric issues with Comsol, the simulation could not be done directly with these values. Comsol 4.1 does not assume that the boundary will move parallel to the *z*-axis. Instead the intersection point of the boundary with the membrane gets fixed.

In order to outline this problem we assumed that the initial volume inside the sphere could be simulated with 2D by a quadratic polygon. The polygon was obtained after several tries to get the desired initial volume. Posteriorly, velocity was also corrected with some attempts to achieve the final volume.

The new and corrected velocity equation in *m/h* is:

$$v = 2.082 \times 10^{-6}t - 6.92 \times 10^{-5} \quad (106)$$

It was also created a Piecewise's function in order to control the movement of boundary through the time.

$$pw1 = \frac{1}{0.00183^2}(x - 0.00183)(x + 0.00183) \quad (107)$$

In Comsol, the final expression of velocity for the boundary is:

$$v_b = v \times pw1(r) \quad (108)$$

F.2 Glucose and furfural fermentation

The initial position and final were maintained. This time, the boundary had to travel the same height as in the previous case, but in 20 *h*.

The result for boundary velocity already corrected in COMSOL, in *m/h* is:

$$v = 2.597 \times 10^{-7}t - 2.112 \times 10^{-5} \quad (109)$$

APPENDIX G - Control coefficient

The Control coefficients were calculated based in the Metabolic Control Analysis theory [36]. Keeping the kinetic and diffusion values as reference, a variation of $\pm 10\%$ was calculated.

Through the use of parametric sweep, the values for glucose and xylose consumption rate were obtained.

It was assumed that the relation between each parameter variation and the reaction rate of glucose and xylose could be described by *Eq. (110)* [36][37].

$$C_{\text{parameter}}^{-r_g} = \frac{\partial \ln(-r_g)}{\partial \ln(\text{parameter})} \quad (110)$$

In order to calculate $C_{\text{parameter}}^{-r_g}$, the values of the parameters and the respective values of $-r_g$ and $-r_x$ were plotted in the natural logarithmic form. The slope of the resulting function was obtained.